

## Quadruple Bonding in the Ground and Low-Lying Excited States of the Diatomic Molecules TcN, RuC, RhB, and PdBe

Demeter Tzeli\* and Ioannis Karapetsas

Cite This: *J. Phys. Chem. A* 2020, 124, 6667–6681

Read Online

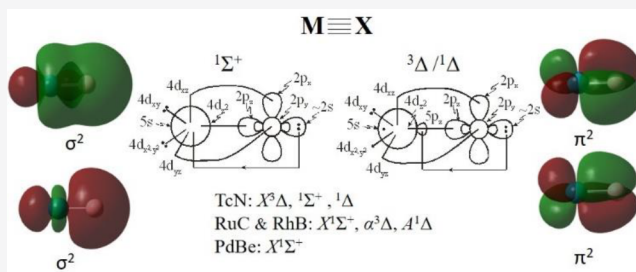
ACCESS |

Metrics &amp; More

Article Recommendations

Supporting Information

**ABSTRACT:** Multiple bonds between atoms are one of the most fundamental aspects of chemistry. Double and triple bonds are quite common, while quadruple bonds are a true oddity and very rare for the main group elements. Identifying molecules containing quadruple bonds is very important and, even more so, determining the necessary requirements for the existence of such bonds. Here we present high-level theoretical calculations on the isoelectronic MX molecules, *i.e.*, TcN, RuC, RhB, and PdBe, showing that such a quadruple bond with main group elements is not that uncommon. We found that quadruple bonds are formed in their ground states  $X^3\Delta$  (TcN) and  $X^1\Sigma^+$  (RuC, RhB, and PdBe) and in the two lowest excited states of TcN ( $^1\Sigma^+$ ,  $^1\Delta$ ), RuC ( $^1,^3\Delta$ ), and RhB ( $^1,^3\Delta$ ). The quadruple bonds consist of two  $\pi$  and two  $\sigma$  bonds:  $(4d_{xz}-2p_x)^2$ ,  $(4d_{yz}-2p_y)^2$ ,  $(4d_z^2-2p_z)^2$ , and  $5s^0 \leftarrow 2s^2$  ( $^1\Sigma^+$ ) or  $5p_z^0 \leftarrow 2s^2$  ( $^1,^3\Delta$ ). Bond lengths, dissociation energies, dipole moments, spectroscopic parameters, and relative energy ordering of the states were calculated *via* multireference and coupled cluster methodology using the aug-cc-pV5Z<sub>X</sub>(-PP)<sub>M</sub> basis sets. We study how the atomic states involved and how the gradual transition from covalent to dative bond, from TcN to PdBe, influence all of the calculated data, such as bond dissociation energies, bond lengths, and relative energy ordering of the states. Finally, we report the requirements for the occurrence of such bonds in molecular systems. All Be, B, C, and N atoms combining with the appropriate second-row transition metal can form quadruple bonds, while they cannot form such bonds with the first-row transition metals.



## 1. INTRODUCTION

The chemical bond is one of the most fundamental concepts in chemistry.<sup>1–3</sup> Multiple bonds between atoms is one of the aspects of chemistry that catches the imagination and attracts great interest among chemists. The multiplicity of a chemical bond is determined by the number of electron pairs that occupy the region between the two bonded atoms in bonding molecular orbitals. Double bonds are quite common, notably in organic compounds, and have been known for over 160 years.<sup>4,5</sup> Triple bonds are found in several frequently encountered molecules such as N<sub>2</sub> and CO. Before 1964, the triple bond was assumed to be the bond of highest multiplicity in any chemical compound. Nowadays, the maximum bond multiplicity is considered to be six and it has been proposed theoretically for the homonuclear diatomic molecules of transition metals, specifically, Cr<sub>2</sub>, Mo<sub>2</sub>, and W<sub>2</sub>,<sup>6</sup> while 5-fold bonding was realized between two Cr(I) centers in a stable compound.<sup>7</sup> However, quadruple bonds are a true oddity and very rare for the main group elements. It should be noted that the quadruple bonds are the bond of highest multiplicity that can form the main group elements. Thus, identifying molecules of main group elements containing quadruple bonds is very important and, even more so, determining the necessary requirements for the existence of such bonds in molecular systems.

Quadruple bonds have been reported on a few occasions. It has been suggested for C<sub>2</sub>, CN<sup>+</sup>, BN, CB<sup>-8</sup>, and RhB,<sup>9</sup> RhB<sup>-9</sup>

Specifically, the exact multiplicity of the bond of the C<sub>2</sub> molecule was placed under scrutiny.<sup>8,10–16</sup> The quadruple bond between Rh and B was reported very recently in a combined experimental and theoretical work. Here we present high-level theoretical calculations showing that such a case is not that uncommon for diatomic molecules containing main group elements and transition metals of the second row. Finally, our ultimate aim is to determine the requirements for the formation of such bonds.

In the present study, we perform high-level multireference configuration interaction and coupled cluster theoretical calculations on the TcN, RuC, RhB, and PdBe molecules. We found that all four molecules present ground states with a quadruple bond and, in the cases of TcN, RuC, and RhB, their two lowest excited states have also quadruple bonds. For all four molecules, we study their bonding and we calculate their dissociation energies, the spectroscopic parameters, and the dipole moments of their lowest in energy states. Additionally, we

Received: April 10, 2020

Revised: July 16, 2020

Published: July 20, 2020



Table 1. Bond Lengths ( $r_e$  (Å)), Binding Energies ( $D_e$  (kcal/mol)), Harmonic Frequencies and Anharmonic Corrections ( $\omega_e$ ,  $\omega_e x_e$  ( $\text{cm}^{-1}$ )), Dipole Moments ( $\mu$  (debye)), and Energy Differences ( $T_e$  (kcal/mol)) of the TcN, RuC, RhB, and PdBe Molecules

state	methods <sup>a</sup>	$r_e$	$D_e$ ( $D_e^d$ ) <sup>b</sup>	$D_e^{gs}$ <sup>b</sup>	TcN	$\omega_e$	$\omega_e x_e$	$\langle \mu \rangle$	$\mu_{\text{FF}}^c$	$T_e$
$X^3\Delta$	MRCISD	1.5966	120.9	109.6		1109.4	5.24	1.743	2.260	0.00
	MRCISD+Q	1.5992	123.3	111.6		1101.0	5.23		2.389	0.00
	RCCSD(T)	1.5946	123.3	110.2		1132.0	4.77		2.391	0.00
	MS-CASPT2 <sup>d</sup>	1.605		121.5		1085		2.38		0.0
$a^1\Sigma^+$	MRCISD	1.5897	149.0(160.0)	93.6		1134.9	4.45	4.615	4.543	16.05
	MRCISD+Q	1.5930	150.8(160.1)	97.1		1124.2	4.46		4.512	14.45
	RCCSD(T)	1.5890	144(153)	94.3		1144.3	4.25		4.483	15.93
	MRCISD	1.5858	129.9	93.5		1146.3	4.84	1.066	1.407	16.03
$b^1\Delta$	MRCISD+Q	1.5880	131.4	96.4		1137.4	4.86		1.671	15.16
	MRCISD	1.6300	90.6	90.6		1018.4	6.17	0.767	1.575	18.97
	MRCISD+Q	1.6291	96.7	96.7		1023.2	6.09		1.371	14.88
	MRCISD	1.6786	97.0	85.5		938.6	4.76	2.795	3.061	24.12
$c^5\Pi$	MRCISD+Q	1.6733	103.1	91.4		945.1	4.68		2.970	20.21
	MRCISD	2.2628		2.32		461.1	3.69	2.985	2.582	107.20
	MRCISD+Q	2.273		0.30		442.3	3.35		2.445	111.24
	MRCISD	2.2191	8.70	-2.59		457.2	8.67	0.958	2.515	112.11
$^9\Sigma^-(2)$	MRCISD+Q	2.193	16.4	4.71		527.7	6.35		3.622	104.36
	MRCISD	1.6018	164.1(174.4)	141.3	RuC	1116.4	4.73	4.205	4.156	0.00
	MRCISD+Q	1.6042	165.5(176.4)	145.9		1109.7	4.73		4.107	0.00
	RCCSD(T)	1.5989	(176.5)	150.1		1130.4	3.82	4.09(14) <sup>e</sup>	3.970	0.00
$a^3\Delta$	expt	1.60790(9) <sup>e,f,g</sup>		154.0 ± 3.0 <sup>f</sup>		1100.0(1.5) <sup>e</sup>	5.3(0.3) <sup>e</sup>			
		1.605485(2) <sup>h</sup>		151.0 ± 3.0 <sup>f</sup>						
		1.616 <sup>i</sup> , 1.634 <sup>m</sup>		145.5 ± 2.5 <sup>f</sup>				4.018 <sup>i</sup> , 4.208 <sup>m</sup>		
	MRCI <sup>k,l</sup>	1.601		129 <sup>j</sup>		1085 <sup>l,m</sup>				
	RCCSD(T) <sup>h</sup>		162.5 <sup>n</sup>			1039.14 <sup>n</sup>	4.75 <sup>n</sup>			
	expt <sup>n</sup>		138.9	138.9		1044.7	4.91	1.466	1.977	2.34
	MRCISD	1.6304	143.8	143.8		1039.8	4.97		2.074	2.13
	MRCISD+Q	1.6332	146.3 ± 2.5 <sup>g</sup>			1038.77(0.39) <sup>e,g,o</sup>	4.64(0.13) <sup>e,o</sup>	1.95(2) <sup>p</sup>	0.217 <sup>f</sup>	
	expt	1.63515 <sup>e,f,o,g</sup>	148.3	125.2		1068.8	5.21	1.122	1.410	16.11
	MRCISD	1.6203	150.5	130.9		1063.1	5.25		1.585	14.98
$A^1\Delta$	MRCISD+Q	1.6230				1032 <sup>e,o,o</sup>				5.84 <sup>e</sup>
	expt	1.6343 <sup>e,o,g</sup>								
	MRCISD	1.6853	134.2	125.4	RhB	943.6	4.43	3.357	3.254	0.0
	MRCISD+Q	1.6873	135.1	126.2		938.3	4.32		3.160	0.0
$X^1\Sigma^+$	RCCSD(T)	1.6872	135.1	126.6		942.1	3.78		2.865	0.0
	CCSD(T) <sup>s</sup>	1.689	130	121						
	expt <sup>t,u,v</sup>	1.69 <sup>s</sup>		112.8 ± 5.0 <sup>u</sup>		920 <sup>s</sup>				
	MS-CASPT2 <sup>v</sup>	1.694	129	121.1 <sup>v</sup>		924		4.54		

Table 1. continued

state	methods <sup>a</sup>	$r_e$	$D_e^a$ ( $D_e^{d,b}$ )	$D_e^{gs,b}$	$\omega_e$	$\omega_e^{x_c}$	$\langle\mu\rangle$	$\mu_{FF}^c$	$T_e$
$a^3\Delta$	MRCISD	1.7645	99.7	99.7	803.7	4.84	1.189	1.807	25.7
	MRCISD+Q	1.7678	101.2	101.2	799.3	4.78		1.871	25.0
	MRCISD	1.7608	102.3(105.9)	91.3	810.0	4.52	1.635	1.326	34.1
	MRCISD+Q	1.7610	102.6(107.4)	93.7	818.3	5.62		1.256	32.5
$X^1\Sigma^+$	MRCISD	1.9123	48.5	48.5	638.1	4.17	1.670	1.219	0.00
	MRCISD+Q	1.9117	52.8	52.8	635.8	4.43		1.007	0.00
	RCCSD(T)	1.9101	49.7	49.7	636.2	2.99		0.786	0.00
$a^3\Sigma^+$	MRCISD	2.0314	32.6(95.5)	12.4	548.4	8.06	1.164	1.037	36.10
	MRCISD+Q	2.0272	37.6(100.6)	17.4	620.2	17.0		0.861	35.37
$b^3\Delta$	MRCISD	2.1533	20.2(83.1)	0.03	463.7	4.20	1.658	1.244	48.46
	MRCISD+Q	2.1466	24.2(87.2)	3.97	462.6	4.56		0.998	48.79
$A^1\Delta$	MRCISD	2.1382	25.4(79.2)	-3.87	490.3	2.63	2.035	1.575	52.37
	MRCISD+Q	2.1324	29.1(83.9)	0.69	487.1	3.13		1.244	52.07

<sup>a</sup>Internally contracted MRCI; +Q refers to the multireference Davidson correction. <sup>b</sup> $D_e^d$ , adiabatic dissociation energy;  $D_e^d$ , diabatic dissociation energy;  $D_e^{gs}$ , dissociation energy with respect to the ground state products. <sup>c</sup>Ground state products  $\mu_{FF}^c = \partial E / \partial R_e$ . <sup>d</sup>Reference 18; MS-CASPT2/4 $\zeta$ -ANO-RCC. <sup>e</sup>Reference 25. <sup>f</sup>Reference 26. <sup>g</sup> $R_{0p}$ ,  $D_0$  values. <sup>h</sup>Reference 34;  $R_e$ . For RCCSD(T) method, SFX2C-1e/CCSD(T)/unc-ANO-RCC level. <sup>i</sup>Reference 21. <sup>j</sup>Reference 22. <sup>k</sup>Reference 30. <sup>l</sup>Reference 28; MRCI/[11s9p5d2f]<sub>Rd</sub>[4s3p1d]<sub>C</sub>. <sup>m</sup>Reference 29; using RECPs: (Ss4p4d2f<sub>Rd</sub>14s4p2d<sub>C</sub>). In parentheses, MRCISD+Q. <sup>n</sup>Reference 23; the state has not been identified as a  $\Sigma^+$  or a  $\Delta$  state. <sup>o</sup>Reference 19 and 20. <sup>p</sup> $\Delta G_{1/2}$ . <sup>q</sup>Reference 24. <sup>r</sup>Reference 31; 1.95(2) for [0.1]<sup>3</sup> $\Delta_3$  and 1.86(2) debye for [0.9]<sup>3</sup> $\Delta_2$ . <sup>s</sup>Reference 9; CCSD(T)/aug-cc-pVQZ<sub>B</sub>(-PP<sub>Rh</sub>). <sup>t</sup>Reference 36. <sup>u</sup>Reference 35;  $D_0$  values. <sup>v</sup>Reference 37;  $D_0$  values. <sup>w</sup>Reference 39; MS-CASPT2/4 $\zeta$ -ANO-RCC.

present a relative energy diagram of about 38–51 states of each molecule. Note that the PdBe molecule has not been studied before. Previous theoretical and experimental data on the TcN,<sup>17,18</sup> RuC,<sup>17,19–34</sup> and RhB<sup>9,17,35–39</sup> molecules are discussed below, and they are summarized in Table 1 along with our results.

**Previous Studies.** There are two theoretical studies on the diatomic TcN molecule in 2009, a DFT<sup>17</sup> and a CASPT2<sup>18</sup> study. Borin and Gobbo<sup>18</sup> calculated 13 electronic states of TcN at the MS-CASPT2/4 $\zeta$ -ANO-RCC level of theory including also scalar relativistic effects. They calculate the ground state, X<sup>3</sup> $\Delta$  state, and three out of four lowest in energy states, <sup>3</sup> $\Sigma^-$ , <sup>5</sup> $\Pi$ , and <sup>1</sup> $\Delta$  states. A triple bond is found in X<sup>3</sup> $\Delta$ , <sup>3</sup> $\Sigma^-$ , and <sup>1</sup> $\Delta$  states previously, and a double bond in <sup>5</sup> $\Pi$ . The bonding in X<sup>3</sup> $\Delta$  and <sup>1</sup> $\Delta$  states was considered as a triple one because the 1 $\sigma$  MO was classified essentially as a 2s lone pair.<sup>18</sup>

The RuC molecule has attracted researchers' interest.<sup>17,19–34</sup> Its spectrum has been measured for the first time in 1965.<sup>20</sup> Data of the X<sup>1</sup> $\Sigma^+$  state and of the <sup>1</sup> $\Pi$ , <sup>1</sup> $\Delta$ , and <sup>3</sup> $\Delta$  states have been obtained *via* mass spectroscopy,<sup>24</sup> resonant two-photon ionization spectroscopy,<sup>26</sup> dispersed fluorescence spectroscopy,<sup>25</sup> optical spectroscopy,<sup>33</sup> rotational spectroscopy,<sup>34</sup> and high-resolution laser-induced fluorescence spectroscopy.<sup>30,31</sup> The dissociation energy of the ground state was determined at 151.0  $\pm$  3.0,<sup>22</sup> 154.0  $\pm$  3.0,<sup>21</sup> and 145.5  $\pm$  2.5 kcal/mol<sup>26</sup> and the bond length at R<sub>c</sub> = 1.605485(2) Å<sup>34</sup> and R<sub>0</sub> = 1.60790(9) Å.<sup>25,26</sup> Finally, the dipole moments of the ground X<sup>1</sup> $\Sigma^+$  state and of the <sup>1</sup> $\Pi$ , <sup>3</sup> $\Pi$ , and <sup>3</sup> $\Delta$  excited states have been measured *via* high-resolution laser-induced fluorescence spectroscopy where the Stark shifts were analyzed,<sup>30,31</sup> *i.e.*, 4.09(14) debye<sup>30</sup> for X<sup>1</sup> $\Sigma$ . The first theoretical calculation on RuC was by Shim and Gingerich in 1985<sup>27</sup> *via* configuration interaction (CI). Then, they calculated some low-lying triplets and singlets states *via* CI<sup>24</sup> and multireference configuration interaction (MRCI).<sup>24,28</sup> Guo and Balasubramanian<sup>29</sup> calculated 29 states *via* first-order configuration interaction (FOCI) using relativistic effective core potentials. For the ground state, Wang *et al.*<sup>34</sup> used the spin-free exact two-component theory and it is a one electron variant relativistic approach at the CCSD(T) level of theory; a thorough discussion of the electron correlation effects was presented. Finally, RuC has been calculated *via* the density functional theory (DFT).<sup>17,32</sup> The chemical bonds in all three lowest lying states were considered as triple bonds composed of one  $\sigma$  and two  $\pi$  bonds.<sup>28</sup>

The first experimental study on RhB was in 1970, where the dissociation energy of the ground state, X<sup>1</sup> $\Sigma^+$ , was measured *via* mass spectroscopy at 112.8  $\pm$  5.0 kcal/mol.<sup>35</sup> In 2006, its bond length was measured at 1.69 Å, by laser-induced fluorescence spectrum.<sup>36</sup> In 2019, the dissociation energies of a series of transition metal borides were measured *via* resonant two-photon ionization spectroscopy;<sup>37</sup> and the dissociation energy of the ground state, X<sup>1</sup> $\Sigma^+$ , was measured at 121.1 kcal/mol with respect to the ground state products. Experimentally, the excited states <sup>1</sup> $\Pi$  and <sup>2</sup> $\Sigma^+$  have been also measured.<sup>36,38</sup> The first theoretical study was in 2008, where 11 states, singlet and triplet states, were calculated by the MS-CASPT2/4 $\zeta$ -ANO-RCC methodology<sup>39</sup> including also scalar relativistic effects. In 2009, it was studied *via* the DFT(B3LYP/LANL2DZ) methodology.<sup>17</sup> Finally, very recently in 2020, Cheung *et al.*<sup>9</sup> studied the ground state of RhB<sup>-</sup> and RhB *via* photoelectron spectroscopy and CCSD(T)/aug-cc-pVQZ<sub>B</sub>(-PP<sub>Rh</sub>) and they concluded that the bond in both molecules is a quadruple one, while all previous theoretical and experimental studies considered the bond in the ground state of

RhB as a triple one, because the 1 $\sigma$  MO was classified essentially as a 2s lone pair.<sup>9</sup>

## 2. BASIS SETS AND METHODS

For the Be, B, C, and N atoms, the correlation consistent basis sets of Dunning *et al.*<sup>40–42</sup> aug-cc-pV5Z, (15s,9p,5d,4f,3g,2h)  $\rightarrow$  [7s,6p,5d,4f,3g,2h], and for second row transition metal Tc, Ru, Rh, and Pd atoms, the Peterson *et al.*<sup>43</sup> correlation consistent basis sets, *i.e.*, aug-cc-pV5Z-PP, (17s,14p,12d,5f,4g,3h,2i)  $\rightarrow$  [8s,8p,7d,5f,4g,3h,2i], were chosen. The latter employ accurate core relativistic pseudopotentials for the 1s<sup>2</sup>2s<sup>2</sup>2p<sup>6</sup>3s<sup>2</sup>3p<sup>6</sup> electrons and treat the 4s<sup>2</sup>4p<sup>6</sup>(5s4d)<sup>7–10</sup> electrons of the transition metal atoms in the *ab initio* calculation. Thus, the contracted basis sets employed here consist of a total of 324 spherical Gaussian-type one electron functions.

At first, a complete active space self-consistent field (CASSCF) calculation was carried out by allotting the 12 “valence” electrons, namely, (5s4d)<sup>7–10</sup> and (2s2p),<sup>2–5</sup> to 10 valence orbitals, *i.e.*, six (5s4d) + four (2s2p) orbitals of the TcN, RuB, RhB, and PdBe molecules. In total 51 (TcN), 38 (RuC), 39 (RhB), and 39 (PdBe) states at the CASSCF level of theory were calculated. Then for the lowest in energy states the multi-reference configuration interaction + single + double excitations (MRCISD) method was employed.<sup>44</sup> The Davidson correction (+Q) was also included in the icMRCISD energy (icMRCISD +Q).<sup>45</sup> The MRCISD spaces range from 13  $\times$  10<sup>6</sup> (<sup>9</sup> $\Sigma^-$ ) to 1089  $\times$  10<sup>6</sup> (A<sup>3</sup> $\Sigma^+$ ) CSFs. By applying the internal contraction approximation (icMRCI),<sup>44</sup> the size of the CI spaces is reduced by more than an order of magnitude, thus making the computations tractable.

Additionally, the restricted coupled cluster + singles + doubles + perturbative triples (RCCSD(T))<sup>46</sup> single reference method was also employed for the ground states X<sup>1</sup> $\Sigma^+$  of RuC, RhB, and PdBe and for X<sup>3</sup> $\Delta$  and <sup>1</sup> $\Sigma^+$  for TcN to confirm the MRCI results. In all RCCSD(T), the 2s2p electrons of Be–N and the 4d5s electrons of the Tc–Pd atoms were correlated. The RCCSD(T) spaces is 1.3  $\times$  10<sup>6</sup> CSFs. In order to evaluate our RCCSD(T), which is a single-reference method, we checked the single ( $t_1$ ) and the double ( $t_2$ ) amplitudes and the  $T_1$  diagnostic. We found that in all calculations of the present work the  $t_1$  and  $t_2$  amplitudes were very small. In most cases, they were smaller than 0.05. Moreover, the  $T_1$  diagnostic is about 0.03 or less in all calculations. These small values of  $t_1$  and  $t_2$  amplitudes and  $T_1$  diagnostic indicate that the single-reference RCCSD(T) method is an appropriate method for the calculated states.

All calculations were done under C<sub>2v</sub> symmetry constraints; however, the CASSCF wave functions possess correct angular momentum symmetry, *i.e.*, | $\Lambda$ | = 0 ( $\Sigma^\pm$ ), 1 ( $\Pi$ ), 2 ( $\Delta$ ), 3 ( $\Phi$ ), 4 ( $\Gamma$ ), and 5 ( $H$ ). This means that  $\Pi$ ,  $\Phi$ , and  $H$  states are linear combinations of B<sub>1</sub> and B<sub>2</sub> symmetries,  $\Delta$  and  $\Gamma$  are combinations of A<sub>1</sub> and A<sub>2</sub> symmetries, whereas  $\Sigma^+$  and  $\Sigma^-$  correspond to A<sub>1</sub> and A<sub>2</sub> species, respectively. Of course, MRCI wave functions do not display in general pure spatial angular momentum symmetry but A<sub>1</sub> for  $\Sigma^+$  and  $\Delta$ , A<sub>2</sub> for  $\Sigma^-$  and  $\Delta$ , and B<sub>1</sub> (or B<sub>2</sub>) for  $\Pi$  states.

For all states, potential energy curves (PECs) have been plotted at the CASSCF and MRCISD levels of theory. It should be noted that most of the calculated states do not correlate in the ground atomic states. Additionally, in many cases they present avoided crossings; as a result, the *in situ* atoms in the minimum are not the same with the correlated ones. Thus, the dissociation energies,  $D_e$ , of all states are calculated with respect to the ground atomic states ( $D_e^{\text{gs}}$ ), with respect to the adiabatic

products ( $D_e^a$ ), and with respect to diabatic products ( $D_e^d$ ). Furthermore, the relative energy ordering at all used levels, *i.e.*, CASSCF, MRCISD, MRCISD+Q, and RCCSD(T), are computed. Finally, at the MRCISD, MRCISD+Q, and RCCSD(T) levels, the spectroscopic constants and dipole moments are reported. The dipole moments are calculated as expectation values ( $\langle\mu\rangle$ ) and by the finite-field method ( $\mu_{FF}$ ).<sup>47,48</sup> Comparing calculated values with experimental ones, it has been found that the finite-field method is to be preferred for the calculation of dipole moments.<sup>48</sup> It is reasonable that the finite-field method give better results than expectation values because the MRCISD calculations have truncated spaces, *i.e.*, the calculations are not full CI. It should be noted that spin-orbit effects are not needed to be considered given that accurate core relativistic pseudopotentials are employed and only 15–18 electrons of the transition metal atoms are treated in the *ab initio* calculations.

The bonding of the lowest in energy states is analyzed, and it is depicted pictorially *via* a valence bond Lewis (vbL) diagram<sup>49</sup> and *via* 3D contour plots of the valence molecular orbitals (MO). Note that the vbL diagrams provide a compact representation of the 3D valence MO. The bond order is the number of chemical bonds between the atoms. A whole bond corresponds to a pair of electrons, while a half-bond corresponds to a bond with one electron. It should be noted that Mulliken, NBO, and CMS population analyses have been carried out; however, while all three analyses confirm the bonding, big differences among the three analyses are observed at the total charge of metal; namely, the Mulliken analysis provides more negative charged metals while CMS more positive charged metals, and the NBO charges are between them; see the Supporting Information (SI). Note also that the use of nonaugmented basis set reduces slightly the charge of the metals only up to 0.15  $e^-$ . The electron charge transfer corresponds to the part of an electron that is transferred from one atom to another in the molecule with respect to the atomic species. In order to check the DFT methodology, the TPSSH<sup>50</sup> functional has been used in conjunction with the aug-cc-pV5Z<sub>X</sub>, aug-cc-pV5Z-PP<sub>M</sub> basis set for the lowest singlets and triplets states of the molecules. The DFT calculations were carried out *via* Gaussian 16.<sup>51</sup> All CASSCF, MRCI, and RCCSD(T) calculations were carried out with the MOLPRO<sup>52</sup> suite of codes.

### 3. RESULTS AND DISCUSSION

**TcN.** At first we calculated 51 states *i.e.*, singlet, triplet, quintet, septet, and nonet  $\Sigma^+$ ,  $\Sigma^-$ ,  $\Pi$ ,  $\Delta$ ,  $\Phi$ ,  $\Gamma$ , and H states at CASSCF/aug-cc-pV5Z<sub>N</sub>(-PP)<sub>Tc</sub>. The ground states of Tc ( $^6S$ ,  $5s^24d^5$ ) and N ( $^4S$ ) give rise to a total of four molecular states, *i.e.*,  $^{3,5,7,9}\Sigma^-$ . The first excited state of Tc ( $^6D$ ,  $5s^14d^6$ ), the second ( $^4D$ ,  $5s^14d^6$ ), the third ( $^4P$ ,  $5s^14d^6$ ), and the fourth ( $^4F$ ,  $4d^7$ ) combined with the ground state of N ( $^4S$ ) give rise to a total of 12 ( $^{3,5,7,9}\Delta$ ,  $\Pi$ ,  $\Sigma^-$ ), 12 ( $^{1,3,5,7}\Delta$ ,  $\Pi$ ,  $\Sigma^-$ ), 8 ( $^{1,3,5,7}\Pi$ ,  $\Sigma^+$ ) and 16 ( $^{1,3,5,7}\Phi$ ,  $\Delta$ ,  $\Pi$ ,  $\Sigma^+$ ) molecular states. Their relative energy levels of the 51 states are given in Figure 1. The calculated singlet, triplet, quintet, septet, and some of the nonet states correlate adiabatically to the ground states of N ( $^4S$ ) + five atomic states of Tc, *i.e.*,  $^6S$ ,  $^6D$ ,  $^4D$ ,  $^4P$ , and  $^4F$ . Their PECs are plotted in Figures S1–S5 of the Supporting Information. The energy separation of the atomic states of Tc are given in Table S1 of the SI. Our data are in very good agreement with the experimental ones.<sup>53</sup>

Then, we calculated at MRCISD/aug-cc-pV5Z<sub>N</sub>(-PP)<sub>Tc</sub> the lowest in energy states,  $X^3\Delta$ ,  $^1\Sigma^+$ ,  $^3\Sigma^-$ ,  $^5\Pi$ , and  $^1\Delta$ . These states,

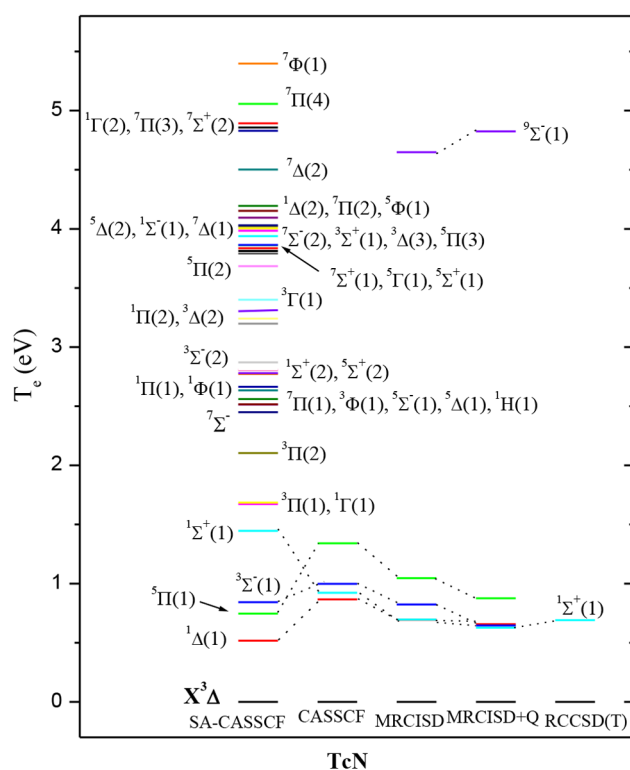


**Figure 1.** Relative energy levels ( $T_e$ ) of 43 states of the TcN molecule at different levels of theory using the aug-cc-pV5Z<sub>N</sub>(-PP)<sub>Tc</sub> basis set. Repulsive nonet states are not plotted.

except  $^1\Sigma^+$ , have been calculated before by Borin and Gobbo.<sup>18</sup> The  $^1\Sigma^+$  state is calculated here for the first time, it is energetically degenerate with the  $^5\Pi$  and  $^1\Delta$  states, and it is calculated here as the first excited state. However, the interesting point about the  $^1\Sigma^+$  state is that it presents a quadruple bond as the  $X^3\Delta$  and  $^1\Delta$  states do. Moreover, RCCSD(T) calculations were carried out for both  $X^3\Delta$  and  $^1\Sigma^+$  states. Finally, we calculated also two  $^9\Sigma^-$  states at MRCISD/aug-cc-pV5Z<sub>N</sub>(-PP)<sub>Tc</sub>. The potential energy curves of the  $X^3\Delta$ ,  $^1\Delta$ ,  $^3\Sigma^-$ ,  $^5\Pi$ , and  $^1\Sigma^+$  states at the MRCISD level are depicted in Figure 2. The ground state is a  $X^3\Delta$  state, and above it, there are three close

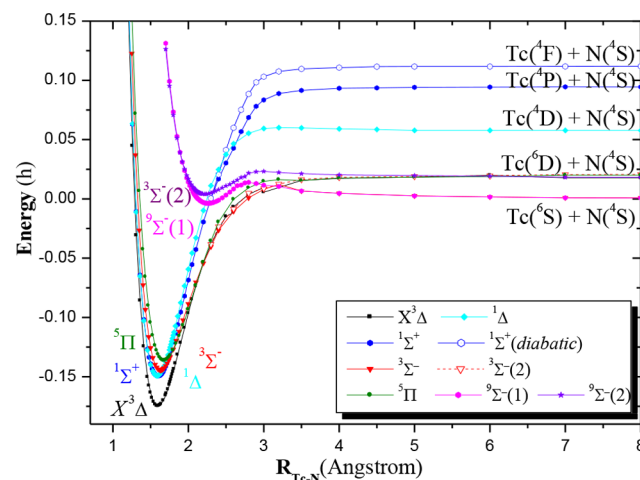
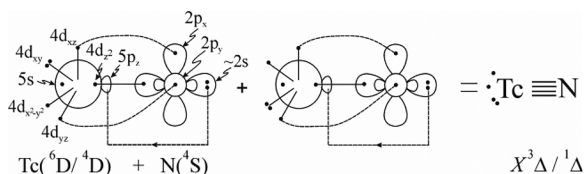


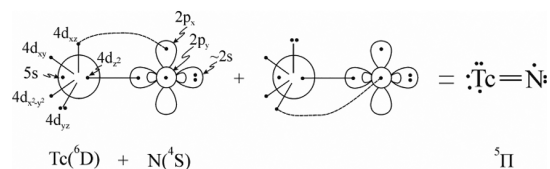
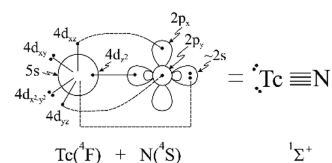
**Figure 2.** MRCISD/aug-cc-pV5Z<sub>N</sub>(-PP)<sub>Tc</sub> potential energy curves of the TcN molecule.

lying in energy states, *i.e.*,  $^1\Sigma^+$ ,  $^1\Delta$ , and  $^3\Sigma^-$ , lying at 14.5 (15.9), 15.2, and 14.9 kcal/mol at the MRCI+Q (RCCSD(T)) level of theory; see Table 1. The three excited states are energetically degenerate, lying within 0.7 kcal/mol, so any of them could be the first excited state.

The ground state,  $X^3\Delta$ , and the low-lying excited state,  $^1\Delta$ , present no avoided crossings, and they correlate to  $\text{Tc}(^6\text{D}, 5s^1 4d^6) + \text{N}(^4\text{S})$  and  $\text{Tc}(^4\text{D}, 5s^1 4d^6) + \text{N}(^4\text{S})$ , respectively, *i.e.*, first and second excited states of Tc. Both states have a quadruple bond. Two  $\pi$  bonds,  $4d_{xz}^1 - 2p_x^1 [0.62(4d_{xz})_{\text{Tc}} + 0.69(2p_x)_{\text{N}}]$  and  $4d_{yz}^2 \rightarrow 2p_y^0 [0.62(4d_{yz})_{\text{Tc}} + 0.69(2p_y)_{\text{N}}]$ , and two  $\sigma$  bonds,  $5p_z^0 \leftarrow 2s^2 [1\sigma \approx -0.37(5p_z)_{\text{Tc}} + 0.91(2s)_{\text{N}}]$  and  $4d_z^1 - 2p_z^1 [2\sigma \approx 0.72(4d_z)_{\text{Tc}} - 0.75(2p_z)_{\text{N}}]$ , are formed; see the vbL diagram below and the 3D plots of valence molecular orbitals (MOs) in Figure S20 of SI. The bond lengths of the  $X^3\Delta$  and  $^1\Delta$  states are 1.599 (1.595) and 1.588 Å, respectively, at the MRCI+Q (RCCSD(T)) level of theory. The binding energies of the two states with respect to their correlated products are 123.3 (123.3) and 131.4 kcal/mol, respectively (see Table 1); the  $^1\Delta$  state presents the largest value. Finally, it should be noted that the  $1\sigma$  bond is not as strong as in the case of  $^1\Sigma^+$  (see below), where the empty orbital is the 5s. As a result, the binding energy in the  $^3,^1\Delta$  state is about 35 kcal/mol less than in the  $^1\Sigma^+$  state; see below.

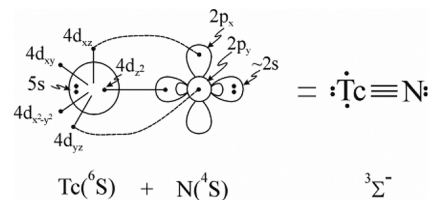


The  $^1\Sigma^+$  state has not been calculated before. It correlates to  $\text{Tc}(^4\text{P}, 5s^1 4d^6) + \text{N}(^4\text{S})$ , *i.e.*, third excited state of Tc. The  $^1\Sigma^+$  state presents an avoided crossing at about 2.3 Å with the  $^1\Sigma^+(2)$  state, which correlates to  $\text{Tc}(^4\text{F}, 4d^7) + \text{N}(^4\text{S})$ , the fourth excited state of Tc. As a result, the  $^1\Sigma^+$  state in the minimum has the Tc atom at its fourth excited state  $^4\text{F}$ .  $\text{Tc}(^4\text{F})$  forms four bonds with the N atom. Analytically, two  $\pi$  bonds,  $4d_{xz}^1 - 2p_x^1 [0.60(4d_{xz})_{\text{Tc}} + 0.71(2p_x)_{\text{N}}]$  and  $4d_{yz}^2 \rightarrow 2p_y^0 [0.60(4d_{yz})_{\text{Tc}} + 0.71(2p_y)_{\text{N}}]$ , and two  $\sigma$  bonds,  $5s^0 \leftarrow 2s^2 [1\sigma \approx 0.21(5s)_{\text{Tc}} - 0.19(5p_z)_{\text{Tc}} + 0.94(2s)_{\text{N}}]$  and  $4d_z^1 - 2p_z^1 [2\sigma \approx 0.71(4d_z)_{\text{Tc}} - 0.75(2p_z)_{\text{N}}]$ , are formed; see vbL diagram below and valence molecular orbitals plots in Figure S20 of the SI. It should be noted that there is a  $2s2p_z$  hybridization in N and a  $5s5p_z$  hybridization in Tc. The four bonds result in binding energies of 160.1 (158.1) [97.1] kcal/mol at the MRCISD+Q level of theory with respect to diabatic (adiabatic) [ground state] products; see Table 1. The bond length is short, 1.593 Å, due to the presence of the quadruple bond. It should be noted that the  $^1\Sigma^+$  state has the largest value of the dipole moment among the lowest in energy states, *i.e.*, 4.51 (4.48) debye at MRCI+Q (RCCSD(T)) level of theory.



The  $^5\Pi$  state correlates to  $\text{Tc}(^6\text{D}, 5s^1 4d^6) + \text{N}(^4\text{S})$ , and it retains this character to the whole PEC. Two bonds are formed, a  $\sigma$  bond  $[d_z^1(\text{Tc}) - p_z^1(\text{N})]$ , and a  $\pi$  bond,  $[d_{xz}^1(\text{Tc}) - p_x^1(\text{N})]$ . Pictorially the bonding is shown in the preceding vbL diagram. The  $^5\Pi$  state has a dissociation energy of 103.1 kcal/mol and a bond length of 1.673 Å, namely, 0.1 Å larger than the corresponding values of the  $X^3\Delta$ ,  $^1\Delta$ , and  $^1\Sigma^+$  states, which have quadruple bonds.

The  $^3\Sigma^-$  state correlates to  $\text{Tc}(^6\text{S}, 5s^2 4d^5) + \text{N}(^4\text{S})$ . It presents two avoided crossings at 3.2 and 2.3 Å with the  $^3\Sigma^-(2)$  state which correlates to  $\text{Tc}(^6\text{D}) + \text{N}(^4\text{S})$ . As a result, the  $^3\Sigma^-(1)$  state regains the character of the ground state atomic products at shorter  $R$  values around the minimum. Three bonds are formed,  $d_z^1(\text{Tc}) - p_z^1(\text{N})$ ,  $d_{xz}^1(\text{Tc}) - p_x^1(\text{N})$ , and  $d_{yz}^1(\text{Tc}) - p_y^1(\text{N})$  (see the vbL diagram below), which result in a binding energy of 90.6 (96.7) kcal/mol at the MRCISD (MRCISD+Q) level of theory; see Table 1. It should be noted that there is a  $2s2p_z$  hybridization in N and a  $5s5p_z$  hybridization in Tc.



Finally, the two  $^9\Sigma^-$  states correlate to  $\text{Tc}(^6\text{S}, 5s^2 4d^5) + \text{N}(^4\text{S})$  and to  $\text{Tc}(^6\text{D}, 5s^1 4d^6) + \text{N}(^4\text{S})$ . The interesting point about these states is that despite all their valence electrons being parallel, both states have a single  $\sigma$  bond which is formed mainly between the  $2p_z^1$  orbital of N empty  $5p_z$  of Tc. The  $^9\Sigma^-(1)$  is bound only 2.3 kcal/mol with respect to the ground state products, while  $^9\Sigma^-(1)$  and  $^9\Sigma^-(2)$  are bound 13.6 and 8.7 kcal/mol with respect to  $\text{Tc}(^6\text{D}) + \text{N}(^4\text{S})$ ; see Table 1.

**RuC.** Thirty-eight states *i.e.*, singlet, triplet, quintet, and septet  $\Sigma^+$ ,  $\Sigma^-$ ,  $\Pi$ ,  $\Delta$ ,  $\Phi$ , and  $\Gamma$  states were calculated at CASSCF/aug-cc-pV5Z<sub>C</sub>(PP)<sub>Ru</sub>. Their relative energy levels are presented in Figure 3, and the PECs of the 38 states are plotted in Figures S6–S9 of the SI. The states correlated adiabatically to the ground states of  $\text{C}(^3\text{P}) +$  two lowest in energy atomic states of Ru, *i.e.*,  $a^5\text{F}(4d^7(a^4\text{F})5s^1)$  and  $a^3\text{F}(4d^7(a^4\text{F})5s^1)$ . The energy separation of the atomic states of Ru is given in Tables S1–S3 of the SI. Our data are in very good agreement with the experimental ones.<sup>53</sup> Then, we calculated at MRCISD/aug-cc-pV5Z<sub>C</sub>(PP)<sub>Ru</sub> the three lowest in energy states, *i.e.*,  $X^1\Sigma^+$ ,  $a^3\Delta$ , and  $A^1\Delta$  states, and at the RCCSD(T)/aug-cc-pV5Z<sub>C</sub>(PP)<sub>Ru</sub> level of theory the ground state. Their potential energy curves at MRCISD are depicted in Figure 4.

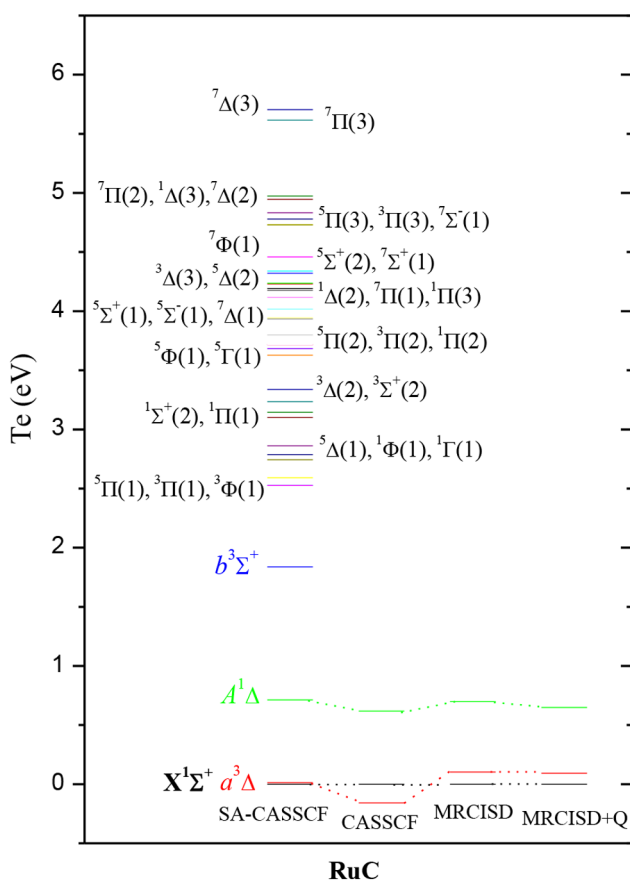
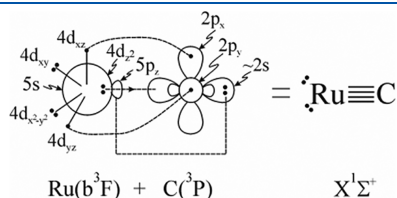


**Figure 3.** Relative energy levels ( $T_e$ ) of 38 states of the RuC molecule at different levels of theory using the aug-cc-pVSZ<sub>C</sub>(-PP)<sub>Ru</sub> basis set.



The  $X^1\Sigma^+$  state correlates to  $\text{Ru}(a^3F; 5s^1 4d^7) + \text{C}(^3P; 2s^2 2p^2)$ .

At 2.7 Å, it suffers from an avoided crossing with the  $1\Sigma^+(2)$  state

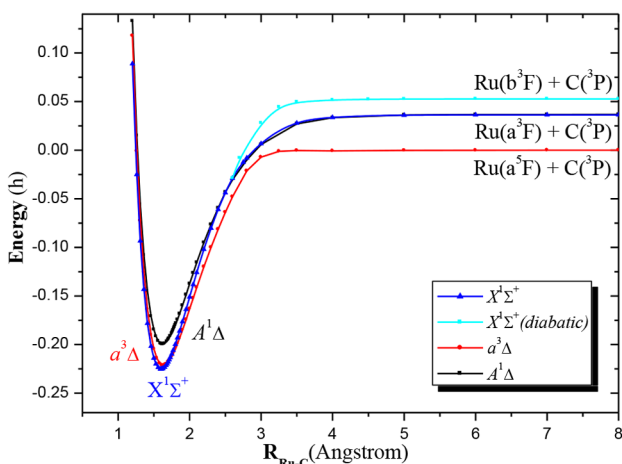
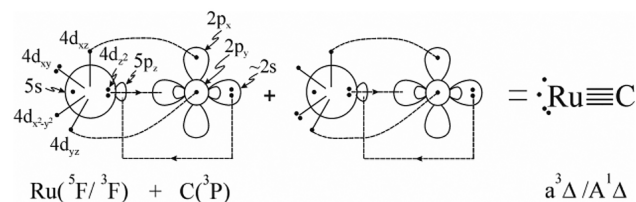


**Figure 4.** MRCI/aug-cc-pVSZ<sub>C</sub>(-PP)<sub>Ru</sub> PECs of RuC. Zero energy corresponds to the atomic ground states products.

which correlates to  $\text{Ru}(b^3F, 4d^8) + \text{C}(^3P; 2s^2 2p^2)$  and as a result the *in situ* atoms in the minimum are  $\text{Ru}(b^3F, 0) + \text{C}(^3P, 0)$ . Four bonds are formed, *i.e.*, two  $\pi$  bonds,  $4d_{xz}^1 - 2p_x^1 [0.74 (4d_{xz})_{\text{Ru}} + 0.58 (2p_x)_{\text{C}}]$  and  $4d_{yz}^2 \rightarrow 2p_y^0 [0.74 (4d_{yz})_{\text{Ru}} + 0.58 (2p_y)_{\text{C}}]$ , and two  $\sigma$  bonds,  $5s^0 \leftarrow 2s^2 [1\sigma \approx 0.35 (5s)_{\text{Ru}} + 0.92 (2s)_{\text{C}}]$  and  $4d_{z^2}^2 \rightarrow 2p_z^0 [2\sigma \approx 0.76 (4d_{z^2})_{\text{Ru}} - 0.65 (2p_z)_{\text{C}}]$ ; see the preceding vbL diagram and plots of MO in Figure S21 of the SI. Finally, comparing the RuC and FeC molecules,<sup>48,54,55</sup> in FeC, where the 2s orbital of the C atom does not form a bond with the empty orbital of Fe, the population in the 2s orbital of C is 0.6  $e^-$  larger than in RuC( $X^1\Sigma^+$ ), where the 2s of C forms a dative bond. This implies that the dipole moment of FeC would be greater than that of RuC for the same state, and this actually happens; see the discussion on dipole moment below.

The quadruple bond results in a short bond length and in a large dissociation energy which both are in excellent agreement with the experimental ones. In more details, the MRCISD+Q(RCCSD(T)) [expt] bond length of the ground state is 1.604 (1.599) [1.605485<sup>34</sup>] Å; see Table 1. The MRCISD+Q and RCCSD(T) dissociation energies are calculated at 176.4 [165.5] {145.9} and 176.5 [150.1] kcal/mol with respect to the diabatic [adiabatic] {ground state} products, *i.e.*,  $\text{Ru}(b^3F) [\text{Ru}(a^3F)] \{\text{Ru}(a^5F)\} + \text{C}(^3P)$  at the MRCISD+Q level in excellent agreement with the experimental  $D_e$  values measured with respect to the ground state products, of  $151.0 \pm 3.0$ <sup>21,22</sup> and  $145.5 \pm 2.5$ <sup>26</sup> kcal/mol. Moreover, the calculated  $\omega_e$ ,  $\omega_e x_e$  and  $\mu$  values are in excellent agreement with the experimental ones, namely, the MRCISD+Q (expt) values are  $\omega_e = 1109.7$  (1100.0<sup>25</sup>)  $\text{cm}^{-1}$ ,  $\omega_e x_e = 4.7$  (5.3<sup>25</sup>)  $\text{cm}^{-1}$ , and  $\mu = 4.107$  (4.09<sup>30</sup>) debye.

The first excited state,  $a^3\Delta$ , is close lying to the ground state; *i.e.*, it is located at 2.1 kcal/mol above the ground  $X^1\Sigma^+$  state. The  $a^3\Delta$  state in the minimum consists of  $\text{Ru}(a^5F; \pm 2, 5s^1 4d^7) + \text{C}(^3P; 0, 2s^2 2p^2)$ , and it correlates to these products. In the minimum, two  $\pi$  bonds are formed,  $4d_{xz}^1 - 2p_x^1 [0.77 (4d_{xz})_{\text{Ru}} + 0.54 (2p_x)_{\text{C}}]$  and  $4d_{yz}^2 \rightarrow 2p_y^0 [0.77 (4d_{yz})_{\text{Ru}} + 0.54 (2p_y)_{\text{C}}]$ ; one  $\sigma$  bond,  $5p_z^0 \leftarrow 2s^2 [1\sigma \approx -0.25 (5p_z)_{\text{Ru}} + 0.95 (2s)_{\text{C}}]$ ; and one  $\sigma$  bond,  $4d_{z^2}^2 \rightarrow 2p_z^0 [2\sigma \approx 0.82 (4d_{z^2})_{\text{Ru}} - 0.66 (2p_z)_{\text{C}}]$ ; see the following vbL diagram and valence MO plots in Figure 21S of the SI. The calculated  $R_e$ ,  $D_e$ ,  $\omega_e$ ,  $\omega_e x_e$ , and  $\mu$  values are in excellent agreement with the experimental values, *i.e.*, the corresponding MRCISD+Q (expt) values are 1.6332 (1.6352<sup>19,20,26</sup>) Å, 143.8 (146.3  $\pm$  2.5<sup>24</sup>) kcal/mol, 1039.8 (1038.77<sup>19,20,25</sup>)  $\text{cm}^{-1}$ , 4.97 (4.64<sup>25</sup>)  $\text{cm}^{-1}$ , and 2.07 (1.95<sup>31</sup>) debye.



Comparing the dipole moment values of RuC and FeC we observe that for the same state their values are similar. The MRCISD (MRCISD+Q) dipole moment value of RuC is found here at 4.16 (4.11) for  $X^1\Sigma^+$  and 1.98 (2.07) debye for  $a^3\Delta$ , in excellent agreement with the measured value by Steimle *et al.*<sup>30,31</sup> of 4.09<sup>30</sup> and 1.95<sup>31</sup> debye, respectively. It should be noted the corresponding calculated [measured] value of FeC( $X^3\Delta$ ) is 2.14<sup>54</sup> [2.36]<sup>55</sup> debye; *i.e.*, FeC presents a larger dipole moment than RuC by 0.2 [0.4] debye in the  $^3\Delta$  states. This happens even though the  $X^3\Delta$  state of FeC presents a

shorter bond distance than the  $a^3\Delta$  state of RuC, by  $\sim 0.04$  Å both theoretically<sup>55</sup> and experimentally,<sup>56</sup> because in the  $\sigma$  frame additional charge is transferred *via* the  $\sigma$  bond from 2s of C to  $5s^0$  of Ru.

The second excited state,  $A^1\Delta$ , is lying 15.0 kcal/mol above the ground state, it correlates to  $\text{Ru}(a^3F, \pm 2; 5s^1 4d^7) + \text{C}(^3P, 0; 2s^2 2p^2)$ , and it preserves this character in all its PECs. The bonding is the same with that of the  $A^3\Delta$  state; the two states differ only in the spin multiplicity, *i.e.*,  $\uparrow\uparrow$  ( $^3\Delta$ ) and  $\downarrow\downarrow$  ( $^1\Delta$ ). The MRCISD+Q calculated  $R_e$ ,  $D_e$ ,  $\omega_e$ , and  $\mu$  values are 1.6230 Å, 150.5 (130.9) kcal/mol (in parentheses is the  $D_e^{\text{gs}}$  value, *i.e.*, with respect to the ground atomic states), 1063.1  $\text{cm}^{-1}$ , and 1.585 D. Comparing the  $A^1\Delta$  and the  $a^3\Delta$  state, the singlet  $\Delta$  state presents shorter bond length by 0.01 Å, larger dissociation energy by 7 kcal/mol, and smaller dipole moment by 0.5 D by the triplet  $\Delta$  state.

**RhB.** Thirty-nine states, *i.e.*, singlet, triplet, quintet, and septet  $\Sigma^+$ ,  $\Sigma^-$ ,  $\Pi$ ,  $\Delta$ ,  $\Phi$ , and  $\Gamma$  states at CASSCF/aug-cc-pV5Z<sub>B</sub>(PP)<sub>Rh</sub> were computed. Their potential energy curves are plotted; see Figures S10–S13 of the SI. The singlet states correlate adiabatically to the atomic states of  $\text{B}(^2P) + \text{Rh}(a^2D, \text{first excited state}; 4d^9)$ , the triplet and quintet states correlate adiabatically to the atomic ground states of  $\text{B}(^2P) + \text{Rh}(a^4F; 4d^8(^3F)5s^1)$ , and the septet states correlate adiabatically to the atomic states of  $\text{B}(^2P) + \text{Rh}(a^4F)/\text{Rh}(a^4P)$ . The energy separation of the atomic states of Rh is given in Tables S1–S3 of the SI, and they are in very good agreement with the experimental ones.<sup>53</sup> Then, we calculated at MRCISD/aug-cc-pV5Z<sub>B</sub>(PP)<sub>Rh</sub> the three lowest in energy states, *i.e.*,  $X^1\Sigma^+$ ,  $a^3\Delta$ , and  $A^1\Delta$  states, and at RCCSD(T)/aug-cc-pV5Z<sub>B</sub>(PP)<sub>Rh</sub> the X state. The relative energy levels of the RhB molecule and the MRCISD PECs are depicted in Figures 5 and 6.

The  $X^1\Sigma^+$  and  $A^1\Delta$  states correlate to  $\text{Rh}(a^2D; 4d^9) + \text{B}(^2P; 2s^2 2p^1)$ , while the first excited state,  $a^3\Delta$ , correlates to the ground state products  $\text{Rh}(a^4F; 5s^1 4d^8) + \text{B}(^2P; 2s^2 2p^1)$ . The  $X^1\Sigma^+$  and  $a^3\Delta$  states retain their asymptotic character in their minimum, while the  $A^1\Delta$  state presents an avoided crossing at about 2.4 Å with an excited  $^1\Delta(2)$  state. As a result the *in situ* atoms in the minimum of  $A^1\Delta$  is  $\text{Rh}(a^2F; 5s^1 4d^8) + \text{B}(^2P; 2s^2 2p^1)$ . The bond length of the ground state is 1.687 Å at both RCCSD(T) and MRCISD+Q levels of theory in excellent agreement with the experimental value of 1.69 Å.<sup>36</sup> The dissociation energy with respect to the asymptotic products  $\text{Rh}(a^2D) + \text{B}(^2P)$  is 135.1 kcal/mol at both RCCSD(T) and MRCISD+Q levels, while the dissociation energy with respect to the ground state products  $\text{Rh}(a^4F) + \text{B}(^2P)$  is 126.6 kcal/mol. The last value is in good agreement with the experimental value of 121.1 kcal/mol.<sup>37</sup> The two lowest excited states,  $a^3\Delta$  and  $A^1\Delta$ , are lying 21.0 and 26.6 kcal/mol above the ground state, and their bond lengths are 1.768 and 1.761 Å; *i.e.*, they are elongated about 0.1 Å compared to the bond length of the  $X^1\Sigma^+$  state. Their dissociation energy with respect to their asymptotic products is 101.2 [ $\text{Rh}(a^4F) + \text{B}(^2P)$ ] and 102.6 [ $\text{Rh}(a^2D) + \text{B}(^2P)$ ], while the dissociation energy of  $A^1\Delta$  with respect to the *in situ* atoms, *i.e.*,  $\text{Rh}(a^2F) + \text{B}(^2P)$  (see diabatic PEC of Figure 6), is 107.4 kcal/mol at the MRCISD+Q level of theory. Our best dipole moments values are obtained *via* finite-field method, *i.e.*, 3.16 ( $X^1\Sigma^+$ ), 1.87 ( $a^3\Delta$ ), and 1.26 ( $A^1\Delta$ ) debye. It should be noted that the finite-field method gives better results than expectation values because the MRCISD+Q calculations have truncated spaces; see below.

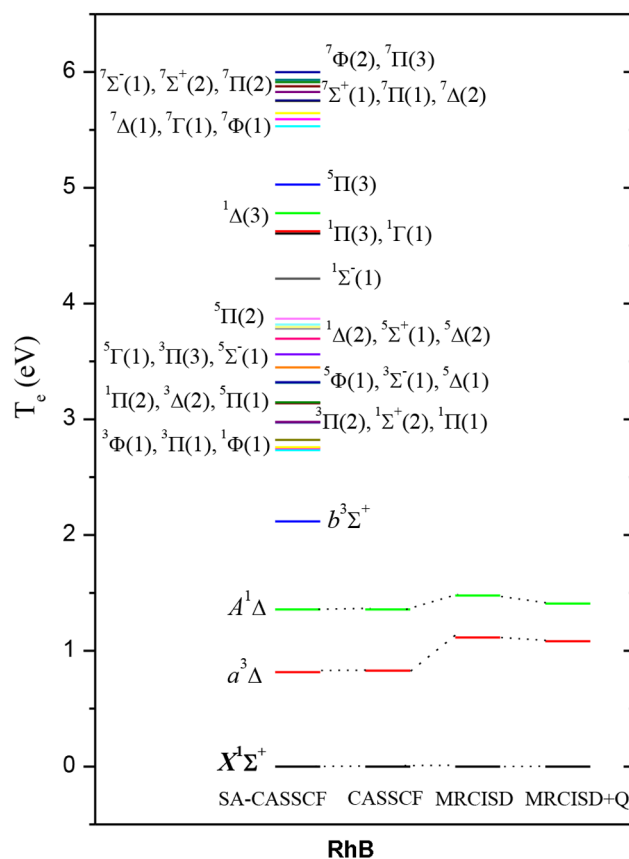


**Figure 5.** Relative energy levels ( $T_e$ ) of 39 states of the RhB molecule at different levels of theory using the aug-cc-pV5Z<sub>B</sub>(-PP)<sub>Rh</sub> basis set.

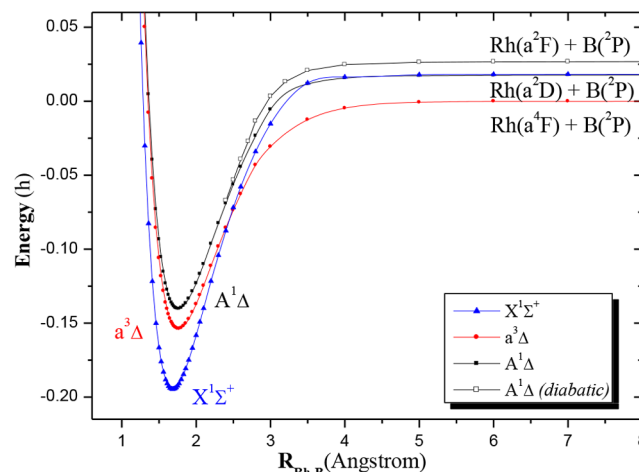
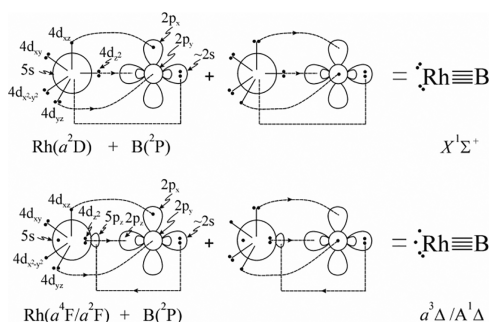


**Figure 6.** MRCI/aug-cc-pV5Z<sub>B</sub>(-PP)<sub>Rh</sub> PECs of RhB. Zero energy corresponds to the atomic ground states products.



The dominant CSFs of the  $X^1\Sigma^+$ ,  $a^3\Delta$ , and  $A^1\Delta$  states and the atomic population analysis are given in Tables S5 and S6 of the SI, while their vbL diagrams are given above and the plots of the MO in Figure S22 of the SI. In the  $X^1\Sigma^+$  state, taking into account the population analysis (see Table S5 of the SI) and molecular orbitals given below, we conclude that four bonds are formed, *i.e.*, two  $\pi$  bonds,  $4d_{xz}^1-2p_x^1$  [ $0.86(4d_{xz})_{Rh} + 0.45(2p_x)_B$ ] and  $4d_{yz}^2 \rightarrow 2p_y^0$  [ $0.86(4d_{yz})_{Rh} + 0.45(2p_y)_B$ ], and two  $\sigma$  bonds,  $5s^0 \leftarrow 2s^2$  [ $1\sigma \approx 0.37(5s)_{Rh} + 0.92(2s)_B$ ] and  $4d_{z^2} \rightarrow 2p_z^0$  [ $2\sigma \approx 0.60(4d_{z^2})_{Rh} - 0.45(2p_z)_B$ ]. In  $a^3\Delta$  and  $A^1\Delta$  states also four bonds are formed, two  $\pi$  bonds ( $4d_{xz}^1-2p_x^1$  and  $4d_{yz}^2 \rightarrow 2p_y^0$ ) and two  $\sigma$  bonds  $5p_z^0 \leftarrow 2s^2$  and  $4d_{z^2} \rightarrow 2p_z^0$ . Note that there is a  $5s5p_z4d_{z^2}$  hybridization in Rh. The two  $\Delta$  states differ only in the spin multiplicity, *i.e.*,  $\uparrow\uparrow$  ( $^3\Delta$ ) and  $\uparrow\downarrow$  ( $^1\Delta$ ). The bonding of  $X^1\Sigma^+$  differs from that of  $a^3\Delta$  and  $A^1\Delta$  to the  $1\sigma^2$  bond, *i.e.*, in  $X^1\Sigma^+$ ,  $1\sigma^2 = 5s^0 \leftarrow 2s^2$ , while in  $a^3\Delta$  and  $A^1\Delta$ ,  $1\sigma^2 = 5p_z^0 \leftarrow 2s^2$ . The first one is stronger because the  $5s$  orbital is lying lower in energy than  $5p_z$ . As a result, the  $X^1\Sigma^+$  state has a shorter bond length by 0.1 Å and stronger dissociation energy by about 30% than the  $a^3\Delta$  and  $A^1\Delta$  states.

It should be noted that very recently Cheung *et al.*<sup>9</sup> studied the ground state of  $RhB^-$  and  $RhB$  *via* photoelectron spectroscopy and CCSD(T)/aug-cc-pVQZ<sub>Be</sub>(-PP)<sub>Rh</sub>, and they concluded that the bond in the ground states of both species is a quadruple one and the  $2s$  of B is involved in the bonding of their ground states. All previous theoretical and experimental studies considered that the bond in the ground state of  $RhB$  is a triple one, because the  $1\sigma$  MO was classified essentially as a  $2s$  lone pair.<sup>9</sup> Here, we conclude that a quadruple bond is formed not only in the ground state of  $RhB$ , in agreement with Cheung *et al.*,<sup>9</sup> but also in the two lowest in energy excited states of the  $RhB$  molecule.

**PdBe.** As far as we know, the PdBe molecule has not been studied before. We calculated 39 states, singlet, triplet, quintet, and septet  $\Sigma^+$ ,  $\Sigma^-$ ,  $\Pi$ ,  $\Delta$ ,  $\Phi$ , and  $\Gamma$  states at CASSCF/aug-cc-pVSZ<sub>Be</sub>(PP)<sub>Pd</sub>. Their PECs are plotted in Figures S14–S17 of the SI. The calculated singlet, triplet, and quintet states correlate adiabatically to the ground ( $^1S$ ) and two lowest in energy excited states ( $^3D$  and  $^1D$ ) of Pd and to the ground ( $^1S$ ) and to the first excited state ( $^3P$ ) of Be. Our calculated energy separation of the atomic states of Pd and Be are in good agreement with the experimental data;<sup>53</sup> see Tables S1–S3 of the SI. The four lowest in energy states of PdBe,  $X^1\Sigma^+$ ,  $a^3\Sigma^+$ ,  $b^3\Delta$ , and  $A^1\Delta$ , are calculated at MRCISD and the X state also at the RCCSD(T) level of theory. The relative energy levels of PdBe and the MRCISD PECs are depicted in Figures 7 and 8.

The atomic ground states of Pd( $1S, 4d^{10}$ ) and Be( $1S$ ) give rise to the  $^1\Sigma^+$  state, which is the ground state of PdBe. The  $X^1\Sigma^+$  state retains the character of the correlated products in the minimum. All used methods, MRCISD, MRCISD+Q, and RCCSD(T), predict the same results, regarding all computational data. The bond length and the dissociation energy of the ground state are 1.912 (1.910) Å and 52.8 (49.7) kcal/mol at the

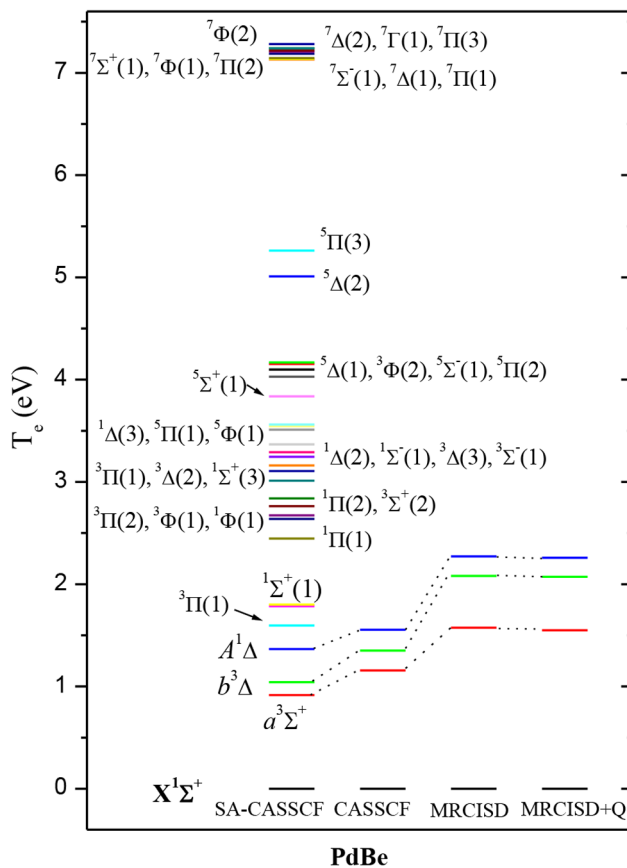


**Figure 7.** Relative energy levels ( $T_e$ ) of 39 states of the PdBe molecule at different levels of theory using the aug-cc-pVSZ<sub>Be</sub>(-PP)<sub>Pd</sub> basis set.

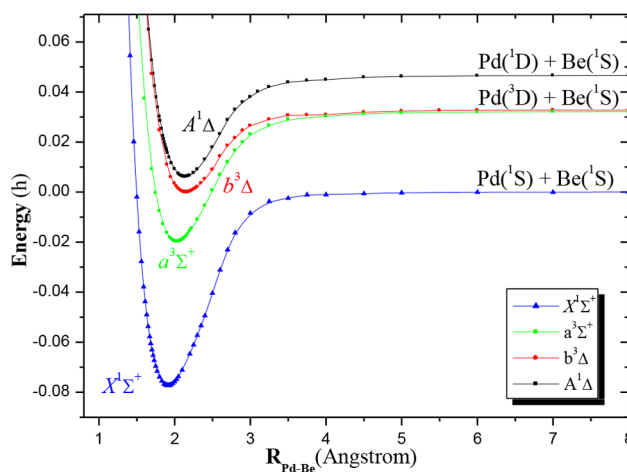
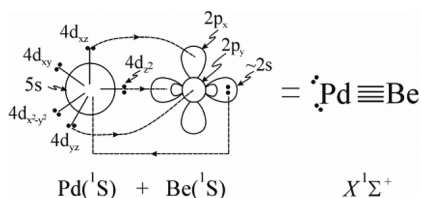


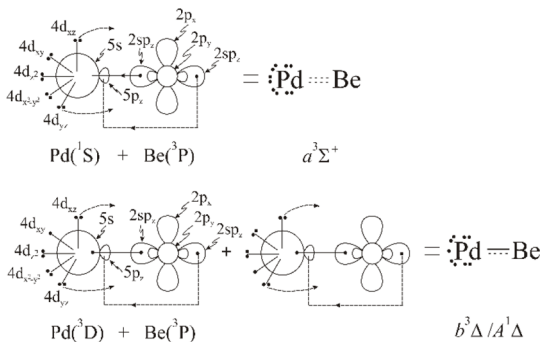
**Figure 8.** MRCI aug-cc-pVSZ<sub>Be</sub>(-PP)<sub>Pd</sub> potential energy curves of the PdBe molecule. Zero energy corresponds to the atomic ground states products.

MRCISD+Q (RCCSD(T)) level of theory. The corresponding  $\omega_e$  and  $\mu$  values are 635.8 (636.2)  $\text{cm}^{-1}$  and 1.007 (0.786) debye. The bonding analysis is given in the following vbL diagram and in Figure 23S of the SI. Two  $\pi$  bonds,  $4d_{xz}^2 \rightarrow 2p_x^0$  [ $0.95(4d_{xz})_{Pd} + 0.27(2p_x)_{Be}$ ] and  $4d_{yz}^2 \rightarrow 2p_y^0$  [ $0.95(4d_{yz})_{Pd} + 0.27(2p_y)_{Be}$ ], and two  $\sigma$  bonds,  $4d_{z^2} \rightarrow 2p_z^0$  [ $1\sigma \approx 0.91(4d_{z^2})_{Pd} + 0.20(5s)_{Pd} - 0.17(5p_z)_{Pd} + 0.50(2p_z)_{Be} - 0.41(5p_z)_{Be}$ ] and  $5s^0 \leftarrow 2s^2$  [ $2\sigma \approx 0.49(5s)_{Pd} + 0.76(2s)_{Be}$ ], are formed. A  $2s2p_z$  hybridization on Be and  $5s5p_z4d_{z^2}$  on Pd are observed. Thus,

four bonds are formed in the ground state as in the cases of the  $X^1\Sigma^+$  states of RhB and RuC and of the  $A^1\Sigma^+$  state of TcN. However, the bond length in PdBe is significantly elongated compared to the other three molecules, *i.e.*, by 0.3 Å (TcN, RuC) and 0.2 Å (RhB) because all four bonds are dative.



The first excited state,  $a^3\Sigma^+$  is lying 35.4 kcal/mol above the ground state, while the following excited states  $b^3\Delta$  and  $A^1\Delta$  are lying 48.8 and 52.1 kcal/mol above the  $X^1\Sigma^+$  state. The  $a^3\Sigma^+$  and  $b^3\Delta$  states correlate to  $\text{Pd}(^3\text{D}) + \text{Be}(^1\text{S})$ , while  $A^1\Delta$  correlates to  $\text{Pd}(^1\text{D}) + \text{Be}(^1\text{S})$ . All three states,  $a^3\Sigma^+$ ,  $b^3\Delta$ , and  $A^1\Delta$ , present avoided crossings at 2.6 Å ( $a^3\Sigma^+$ ,  $b^3\Delta$ ) and 2.8 Å ( $A^1\Delta$ ) with  $^3\Sigma^+(2)$ ,  $^3\Delta(2)$ , and  $^1\Delta(2)$ , respectively, which all correlate diabatically to  $\text{Pd}(^3\text{D}) + \text{Be}(^3\text{P})$  in the  $\Delta$  states and to  $\text{Pd}(^1\text{S}) + \text{Be}(^3\text{P})$  in the  $^3\Sigma^+$  state. The bond lengths of the  $a^3\Sigma^+$ ,  $b^3\Delta$ , and  $A^1\Delta$  states are 2.027, 2.147, and 2.132 Å, and their diabatic (adiabatic) [with respect to the ground atoms] dissociation energies are 100.6 (37.6) [17.4], 87.2 (24.2) [4.0], and 83.9 (29.1) [0.7] kcal/mol. At the minimum of all three states, there is a  $2s2p_z$  hybridization in Be and a  $5s5p_z4d_z^2$  in Pd. The vBL diagrams and MO orbitals (Figure S23 of the SI) that describe the bonds are the following:



**Comparison.** All four MX calculated molecules, TcN, RuC, RhB, and PdBe, are isoelectronic, having 50 electrons. The bond lengths of the  $^1\Sigma^+$  and  $^3\Delta$ ,  $^1\Delta$  states with respect to the increase of the atomic number of the metals are plotted in Figure 9. All used methodologies are in agreement regarding the bond lengths of the calculated states. As the atomic number of the metals increases, the bond lengths of the three states also increases. However, while, for the TcN molecule all three states present similar bond length, the increase of the bond length of the  $\Delta$  states is larger than the bond length of the  $\Sigma^+$  state and the plots of the bond lengths of  $\Sigma^+$  and  $\Delta$  diverge; see Figure 9. The % increase of the bond length from TcN to RuC for  $^1\Sigma^+$  ( $^3\Delta$ ) is 0.7 (2.2), from RuC to RhB is 5.2 (8.5), and from RhB to PdBe is 13.3 (21.40); see Table S7 of the SI. Note that the two  $\Delta$  states present similar bond lengths, with the bond length of the  $^3\Delta$  state being slightly larger, up to 0.01 Å, than the corresponding bond length of the  $^1\Delta$  state. All of these differences in the values of the bond lengths from the one molecule to the other result from the type of bonding. The short bonds of the  $^1\Sigma^+$  states of M–X result from the fact that quadruple bonds are formed in all molecules. However, while in the  $^1\Sigma^+$  states of all M–X a quadruple bond is formed, the bond lengths of the  $^1\Sigma^+$  state is

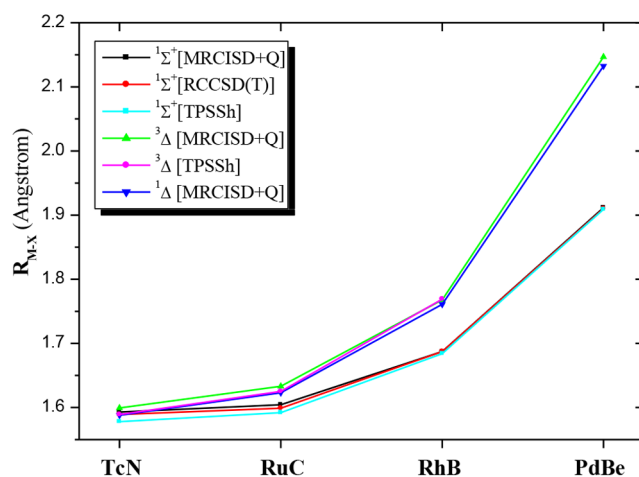


**Figure 9.** Bond length  $R_{\text{M-X}}$  of the  $^1\Sigma^+$ ,  $^3\Delta$ , and  $^1\Delta$  states of the M–X molecules at different levels of theory using the aug-cc-pV5Z<sub>X</sub>(-PP)<sub>M</sub> basis set.

increased with respect to the increase of the atomic number of the metals and the analogous decrease of the atomic number of X. This is attributed to the fact that, while in TcN three bonds are covalent and one bond is dative ( $5s^0 \leftarrow 2s^2$ ), in RuC two bonds are covalent and two are dative, in RhB one bond is covalent and three are dative, and finally in PdBe all four bonds are dative, resulting in a large increase of the bond length in PdBe. In  $\Delta$  states, quadruple bonds are formed in the TcN, RuC, and RhB molecules, while in PdBe one and a half bonds resulting in a significant increase of 21.4% in bond length.

The dipole moments of the  $^1\Sigma^+$  and  $^3\Delta$ ,  $^1\Delta$  states with respect to the increase of the atomic number of the metals are plotted in Figure 10; see also Table 1. The dipole moments were calculated

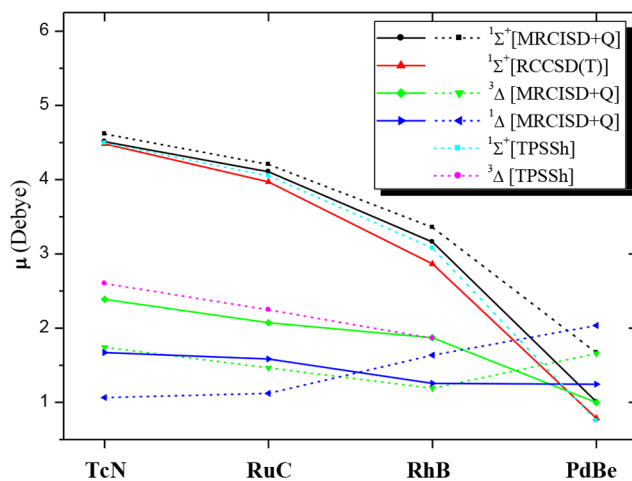


**Figure 10.** Dipole moment ( $\mu$ ) of the  $^1\Sigma^+$ ,  $^3\Delta$ , and  $^1\Delta$  states of the M–X molecules at different levels of theory using the aug-cc-pV5Z<sub>X</sub>(-PP)<sub>M</sub> basis set. Solid lines correspond to values calculated *via* finite field; dotted lines correspond to expectation values.

as expectation values ( $\langle\mu\rangle$ ) and by the finite-field method ( $\mu_{\text{FF}}$ ). Regarding the comparison of the values obtained by the two methods, in some cases both methods predict the same dipole moment, for instance  $^1\Sigma^+$  of TcN and RuC; however, in some cases they differ up to 0.6 D ( $^3\Delta$ , of RhB). Moreover, the trends on dipole moments calculated by the two methods are the same

for the  $^1\Sigma^+$  states but not for the  $\Delta$  states. The differences in the two methods results from the fact the MRCISD method is a truncated CI and not a full CI. We consider that the values obtained by the finite-field method are the best ones; see below and ref 48. In Figure 10, we observe that the increase of the atomic number of the metals results in a significant decrease of the dipole moment of the  $^1\Sigma^+$  state. The dipole moment of the  $^1\Sigma^+$  state of PdBe is decreased by 80% compared to the corresponding value of TcN; see Table S7 of the SI. Regarding the dipole moments of  $\Delta$  states, triplets present larger values than singlets and their values decrease from TcN to RhB by 0.52 (0.42) debye for the  $^3\Delta$  ( $^1\Delta$ ) states, while, in PdBe,  $^1\Delta$  presents a larger dipole moment value than the triplet. The decrease of the values of dipole moments on  $^1\Sigma^+$ ,  $^3\Delta$ , and  $^1\Delta$  states, from TcN to RhB, results from the fact that the difference in electronegativity of the atoms of each molecule is decreased from 2.1 (TcN) to 0.3 (RhB).<sup>57</sup> In the case of PdBe, the small value of the dipole moment results from the significant reduction of the bond length; see above. Finally, it should be noted that the dipole moments of the  $\Delta$  states calculated as an expectation value present an increase from RhB to TcN which is not reasonable, showing that the finite-field method is the best method for the correct calculation of the dipole moment.

The values of dissociation energies  $D_e^{gs}$ ,  $D_e^a$ , and  $D_e^d$  with respect to the molecules have been plotted in Figure 11 and

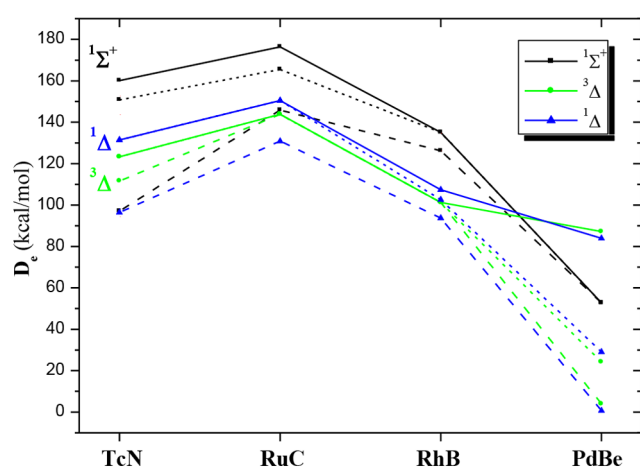


**Figure 11.** Dissociation energies ( $D_e$ ) (diatomic,  $D_e^d$ , solid line; adiabatic,  $D_e^a$ , dotted line; with respect to the atomic ground states,  $D_e^{gs}$ , dashed line) of the  $^1\Sigma^+$ ,  $^3\Delta$ , and  $^1\Delta$  states of the M–X molecules at the MRCISD+Q/aug-cc-pV5Z<sub>X</sub>(-PP)<sub>M</sub> level of theory.

Figure S18 of the SI. Note that in  $^1\Sigma^+$  (TcN, RuC),  $^3\Delta$  (PdBe),  $^1\Delta$  (ThB, PbBe),  $^3\Sigma^+$  (PdBe), the atomic ground states, the correlated atomic states, and the *in situ* atomic states differ; as a result the three  $D_e$  values differ. In  $X^3\Delta$  (TcN),  $^1\Delta$  (TcN, RuC),  $X^1\Sigma^+$  (RhB), and  $^3\Pi$  (TcN) the correlated atoms are the same as those of the *in situ* atoms but they differ from the atomic ground states, *i.e.*,  $D_e^a = D_e^d$ , while, in  $^3\Delta$  (RuC, RhB),  $X^1\Sigma^+$  (PdBe), and  $^3\Sigma^-$  (TcN) states, the *in situ* atoms states are the same with the correlated ones which are the atomic ground states and, thus, the three  $D_e$  values are the same. We observe that all  $D_e$  values increased from TcN to RuC and then they decreased at PdBe; see Figure 11. Specifically, the  $D_e^d$  values of the three states of RuC are larger than the corresponding values of the states of TcN; the increase of the  $D_e^d$  values ranges from 9 to 17% (up to 20 kcal/mol); *i.e.*, the bonding is stronger in RuC. Comparing

the  $D_e^d$  values of the three states of RhB with those of RuC, we observe that the  $D_e^d$  values of RhB are smaller than the corresponding values of the states of RuC by 18% ( $^1\Sigma^+$ ) to 32% ( $^1\Delta$ ). Note that in the  $\Delta$  states of RhB triple bonds are formed, while in RuC quadruple bonds are formed. Regarding charge transfer, the largest ones are calculated for RuC and RhB, while the smallest charge transfer is calculated for TcN and PdBe for different reasons. In TcN, three out of four bonds are covalent, thus less charge transfer occurs than in RuC and RhB which have two and three dative bonds, respectively; while, in PdBe, the bonds are weaker, *i.e.*, all are dative, than the bonds in the other MX molecules.

The harmonic frequencies of the  $^1\Sigma^+$ ,  $^3\Delta$ , and  $^1\Delta$  states of MX are decreased from TcN to PdBe; see Figure 12. The  $\omega_e$  values in

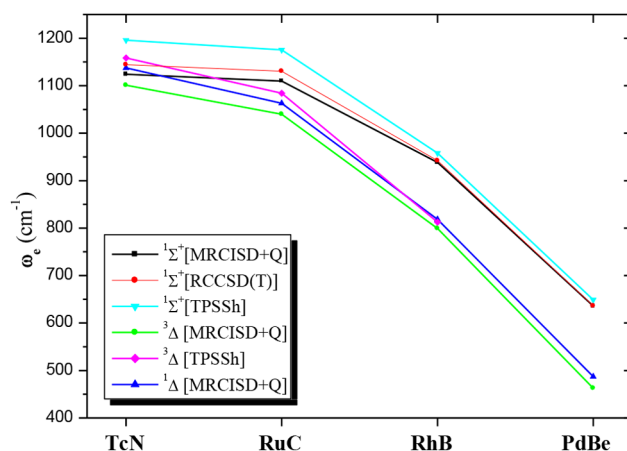


**Figure 12.** Frequencies ( $\omega_e$ ) of the lowest in energy states of the MX molecules at the MRCISD+Q, RCCSD(T), and TPSSh/aug-cc-pV5Z<sub>X</sub>(-PP)<sub>M</sub> levels of theory.

RhB are slightly smaller than the values of TcN, while the corresponding values in PdBe are half those of TcN. Thus, the TcN and RuC molecules are more rigid than RhB, and they are significantly more rigid than PdBe.

The relative energies  $T_e$  of the calculated states of the M–X molecules are depicted in Figure 13 and in Figure S19 of the SI

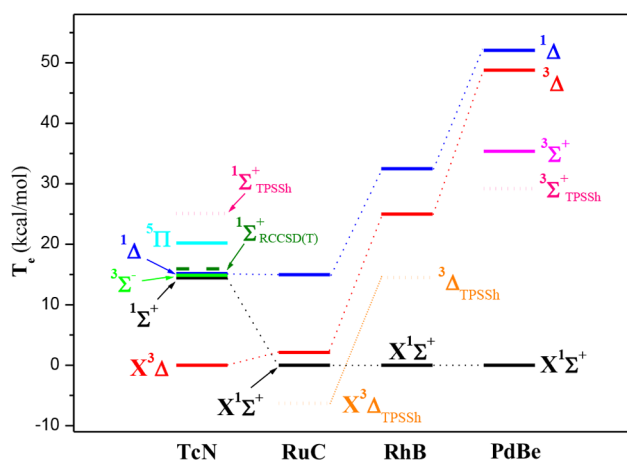


**Figure 13.** Relative energy levels ( $T_e$ ) of the lowest in energy states of the MX molecules with respect to the ground states of MX at the MRCISD+Q (solid lines), RCCSD(T) (dashed lines), and TPSSh (dotted lines)/aug-cc-pV5Z<sub>X</sub>(-PP)<sub>M</sub> levels of theory.

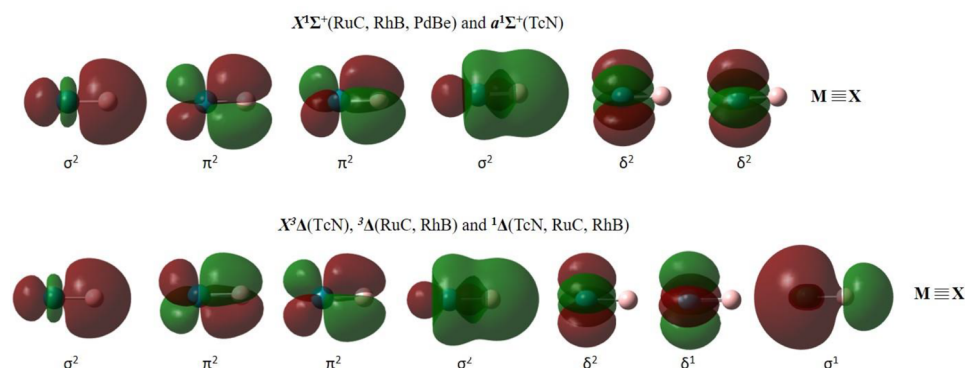


**Figure 14.** Molecular orbitals of the  $^1\Sigma^+$ ,  $^3\Delta$ , and  $^1\Delta$  states presenting quadruple bonds. (The plotted 3D orbital contours correspond to RhB molecule which are the same with the 3D orbital contours of the TcN, RuC, and PdBe; see Figures 20S–24S of the SI.)

from a different point of view. The ground state of TcN is the  $X^3\Delta$  state, while the ground state of RuC, RhB, and PdBe is the  $X^1\Sigma^+$  state at the MRCISD, MRCISD+Q, and RCCSD(T) levels of theory. Note that the DFT methodology does not predict very well the relative energy levels; see below. The PdBe molecule has the largest energy separation between its ground state  $X^1\Sigma^+$  state and the  $^3\Delta$  state, and as the atomic number of M is decreased, also the energy separation is decreased. Thus, in TcN, the ordering of the states is reversed and as a result the ground state of TcN is the  $X^3\Delta$  state; see Figure 12. This happens because of (i) the different multiplicities of the bonds in the two states, *i.e.*, in PdBe,  $X^1\Sigma^+$  (quadruple bond) and  $^3\Delta$  (one and a half) and in RhB, RuC, and TcN,  $X^1\Sigma^+$  and  $^3\Delta$  (quadruple), and (ii) the different types of bonds covalent *versus* dative. Regarding the reverse ordering of the  $^1\Sigma^+$  and  $^3\Delta$  in RuC and TcN, it results from the fact that the energy separation of the Tc atomic states that are involved in the molecular states is bigger than in Ru states. In RuC, the fourth excited state of Ru( $b^3F;4d^8$ ) for  $^1\Sigma^+$  and the ground state of Ru( $a^5F;4d^75s^1$ ) for  $^3\Delta$  are involved; their MRCISD+Q (RCCSD(T)) [expt] energy gap is 1.223 (1.147) [1.092<sup>52</sup>] eV. In TcN, the fourth excited state Tc( $a^5F;4d^7$ ) for  $^1\Sigma^+$  and the first excited state Tc( $a^6D;4d^65s^1$ ) for  $^3\Delta$  are involved; their MRCISD+Q [expt] energy gap is 1.949 [1.926<sup>52</sup>] eV. Thus, the MRCISD+Q [expt] atomic energy of the two metal states in TcN is larger than that in RuC by 0.726 [0.834] eV, and as a result the relative ordering of the diatomic states  $^1\Sigma^+$  and  $^3\Delta$  in RuC and TcN is reversed. A last comment, the energy gap between  $^3\Delta$  and  $^1\Delta$  states in PdBe is the smallest one, while as the atomic number of M is decreased, the energy gap is increased. This also results from the involved M atomic states in the molecules. In PdBe, both  $\Delta$  states contain the same atomic state of Pd, while in the remaining diatomics, the *in situ* atomic states of M differ and their energy difference increases as the atomic number of M is decreased. Their MRCISD+Q [expt<sup>53</sup>] energy gap is 0.593 [0.632] eV for Rh( $^2F\leftarrow^4F$ ), 0.794 [0.782] eV for Ru( $a^3F\leftarrow a^5F$ ), and 0.987 [0.962] eV for Tc( $^4D\leftarrow^6D$ ). It should be noted that theoretical and experimental data are in excellent agreement.

Comparing the different methodologies used here, we observe that MRCISD (MRCISD+Q) and RCCSD(T) methods predict similar data; see Table 1. Comparing the relative energy levels calculated by CASSCF and by SA-CASSCF, we observe that, in the case of RhB, both methods predict the same results in agreement with the MRCI methods. In the case of RuC, the SA-CASSCF method calculates better the relative energy ordering than the CASSCF method; CASSCF reverses the ordering of  $^1\Sigma^+$  and  $^3\Delta$  in disagreement with our MRCI methods; however,

note that both states are close lying, *i.e.*, within 2 kcal/mol at the MRCI level. For the TcN and PdBe molecules, there are energy differences between CASSCF and SA-CASSCF with the MRCI methods. In both molecules, CASSCF seems to be a better method than SA-CASSCF. In TcN, the CASSCF (SA-CASSCF) methods overestimate the relative energy levels less than 6.8 (18.9) kcal/mol, while, in PdBe, they underestimate them less than 16.6 (23.8) kcal/mol. In general, the poorer performance of SA-CASSCF comparing to the CASSCF is due to the large number of states being averaged. Comparing the DFT/TPSSH data with MRCISD (MRCISD+Q) and RCCSD(T) results, we observe that DFT predicts very well the bond lengths and quite well the dipole moments and the harmonic frequencies of all of the  $^1\Sigma^+$ ,  $^3\Delta$ , and  $^1\Delta$  states. In  $D_e^{85}$  values, the largest deviation between DFT and MRCISD+Q or RCCSD(T) are up to  $\pm 15$  kcal/mol. Finally, the relative energy levels of the  $^1\Sigma^+$  and  $^3\Delta$  states are not very well described by the DFT/TPSSH; for TcN the energy gap is significantly overestimated by 74% while, in RhB, is underestimated by 72%. Finally, in RuC,  $^3\Delta$  is calculated as the ground state instead of  $^1\Sigma^+$ . To sum up, for the correct study of diatomic molecules containing second-row transition metals, the use of the multireference configuration interaction or coupled cluster methodology is necessary.

Thus, we have analyzed how the relative energy of the atomic states involved and the gradual transition from covalent to dative bond, from TcN to PdBe, influence all calculated data, such as bond dissociation energies, bond lengths, dipole moments, and relative energy ordering of the states. Regarding the ability of the MX calculated molecules to form quadruple bonds in their ground states and excited states, this results from the fact the transition metals have low lying in energy atomic states having 5s and 5p<sub>z</sub> unoccupied orbitals that can receive electrons *via* dative bonds. It should be noted that the quadruple bond is the bond of the highest multiplicity that can form the main group elements of the second period. From the present study we observe that all Be, B, C, and N atoms combined with the appropriate second-row transition metal can form quadruple bonds. Finally, comparing the first-row transition metals<sup>53,58</sup> with the second row, the first ones have no low lying in energy atomic states, having 4s unoccupied orbitals, and thus, they cannot form quadruple bonds with the main group elements.

#### 4. SUMMARY AND CONCLUSIONS

Multiple bonding attracts great interest. In diatomic molecules, double and triple bonds are found in several frequently encountered molecules; however, quadruple bonds are rare.

For the main group elements, quadruple bonds are the bond of highest multiplicity. The main purpose of the present study is to show that a quadruple bond is not that uncommon and to discuss and explain the requirements for the occurrence of such bonds.

In the present study, we have carried out high-level theoretical calculations on isoelectronic MX molecules, *i.e.*, TcN, RuC, RhB, and PdBe, which all have 50 electrons. We calculated up to 51 states for each molecule, and we plotted their potential energy curves. For the low-lying states, we computed their bond lengths, diabatic and adiabatic dissociation energies, dipole moments, and spectroscopic parameters at the MRCISD (MRCISD+Q) and RCCSD(T) levels. Emphasis is given in the bonding analysis and how it affects all of the calculated data as the metal change.

We found that the ground states of all four molecules have quadruple bonds as clearly shown in Figure 14, reaching dissociation energies up to 176.4 kcal/mol. Additionally, the two lowest excited states of TcN, RuC, and RhB have also quadruple bonds. Namely,  $X^3\Delta$ ,  $a^1\Sigma^+$ , and  $b^1\Delta$  of TcN,  $X^1\Sigma^+$ ,  $A^3\Delta$ , and  $a^1\Delta$  of RuC and RhB, and  $X^1\Sigma^+$  of PdBe have quadruple bonds. The MRCI+Q bond length, the diabatic (adiabatic) [with respect to the ground state] dissociation energy, and dipole moments of the ground states and  $^1\Sigma^+$  of TcN are 1.5930 Å, 160.1 (150.8) [97.1] kcal/mol, 4.512 D for  $a^1\Sigma^+$  (TcN); 1.5992 Å, 123.3 (123.3) [111.6] kcal/mol, 2.389 D for  $X^3\Delta$  (TcN); 1.6042 Å, 176.4 (165.5) [145.9] kcal/mol, 4.107 D for  $X^1\Sigma^+$ (RuC); 1.6873 Å, 135.1(135.1)[126.2] kcal/mol, 3.160 D for  $X^1\Sigma^+$  (RhB); and 1.9117 Å, 52.8 (52.8) [52.8] kcal/mol, 1.007 D for  $X^1\Sigma^+$  (PdBe).

The quadruple bonds of the  $^1\Sigma^+$  states of molecules, *i.e.*, ground state of RuC, RhB, and PdBe and first excited state of TcN, result from the fact that these four transition metals have low-lying atomic states of the type  $5s^04d$ .<sup>7–10</sup> This atomic state is the fourth state for Tc and Ru lying at 2.505 (2.332) and 1.223 (1.131) eV at MRCI+Q (expt<sup>53</sup>), the first excited state for Rh lying at 0.386 (0.342) eV, and the ground atomic state for Pd. In  $^1\Sigma^+$  states of the calculated molecules, additionally to a triple bond (two  $\pi$  and one  $\sigma$  bond) which is commonly formed in molecules containing transition metals, a fourth  $\sigma$  dative ( $5s^0 \leftarrow 2s^2$ ) is formed. In total, in TcN three bonds are covalent and one bond is dative, in RuC two bonds are covalent and two are dative, in RhB one bond is covalent and three are dative, and finally in PdBe all four bonds are dative resulting in an increase of the bond length in PdBe.

In TcN, RuC, and RhB, quadruple bonds are also formed in the  $^3\Delta$  and  $^1\Delta$  states, *i.e.*, in the ground state  $X^3\Delta$  and the second excited state  $b^1\Delta$  of TcN and in the first  $a^3\Delta$  and second  $A^1\Delta$  excited states of RuC and RhB. Both  $\Delta$  states of TcN contain an excited Tc, *i.e.*,  $X^3\Delta$  has a Tc( $^6D, 5s^14d^6$ ; first excited state) and  $b^1\Delta$  has a Tc( $^4D, 5s^14d^6$ ; second excited state). The  $^3\Delta$  state of RuC contains a Ru atom in its ground state ( $^5F, 5s^14d^7$ ) and the  $A^1\Delta$  of RuC has a Ru atom in its first excited state ( $^3F, 5s^14d^7$ ). Similarly, the  $^3\Delta$  state of RhB contains a Rh( $^4F, 5s^14d^8$ ; ground state of Rh) and the  $A^1\Delta$  of RhB has a Rh( $^2F, 5s^14d^8$ ; second excited state of Rh). The two  $\Delta$  states in each molecule differ only by the spin multiplicity, *i.e.*,  $\uparrow\uparrow$  ( $^3\Delta$ ) and  $\downarrow\uparrow$  ( $^1\Delta$ ). As in the  $^1\Sigma^+$  states, additionally to a common triple bond (two  $\pi$  and one  $\sigma$  bond), here a fourth  $\sigma$  dative ( $5p_z^0 \leftarrow 2s^2$ ) is formed. Thus, in TcN three bonds are covalent and one bond is dative, in RuC two bonds are covalent and two are dative, and in RhB one bond is covalent and three are dative.

Finally, we analyze how the relative energy of the atomic states and the gradual transition from covalent to dative bond, from TcN to PdBe, influence all calculated data, such as bond dissociation energies, bond lengths, dipole moments, and relative energy ordering of the states. We conclude that there are two necessary requirements for the occurrence of quadruple bonds: (i) the existence of low-lying atomic states that have low-lying unoccupied orbitals that can receive electrons *via* dative bonds and (ii) atoms with double occupied orbitals that can form dative bonds. The first-row transition metals do not have low-lying atomic states having 4s unoccupied orbitals, and thus, they cannot form quadruple bonds with the main group elements. Finally, we observe that all Be, B, C, and N atoms combining with the appropriate second-row transition metal can form quadruple bonds. To sum up, it is important to analyze the reasons why atoms can form multiple bonds because that will lead to the identification of molecules forming such bonds.

## ■ ASSOCIATED CONTENT

### Supporting Information

The Supporting Information is available free of charge at <https://pubs.acs.org/doi/10.1021/acs.jpca.0c03208>.

Atomic states, energetics, spectroscopic parameters, population analysis, potential energy curves, computational details at CASSCF, MRCISD(+Q), RCCSD(T), and DFT levels of theory (PDF)

## ■ AUTHOR INFORMATION

### Corresponding Author

Demeter Tzeli – Laboratory of Physical Chemistry, Department of Chemistry, National and Kapodistrian University of Athens, Athens 157 84, Greece; Theoretical and Physical Chemistry Institute, The National Hellenic Research Foundation, Athens 11635, Greece; [orcid.org/0000-0003-0899-7282](https://orcid.org/0000-0003-0899-7282); Email: [tzeli@chem.uoa.gr](mailto:tzeli@chem.uoa.gr), [dtzeli@eie.gr](mailto:dtzeli@eie.gr)

### Author

Ioannis Karapetsas – Laboratory of Physical Chemistry, Department of Chemistry, National and Kapodistrian University of Athens, Athens 157 84, Greece

Complete contact information is available at: <https://pubs.acs.org/doi/10.1021/acs.jpca.0c03208>

### Notes

The authors declare no competing financial interest.

## ■ ACKNOWLEDGMENTS

D.T. acknowledges support from the Center for Scalable Predictive methods for Excitations and Correlated phenomena (SPEC), which is funded by the U.S. Department of Energy, Office of Science, Basic Energy Sciences, Chemical Sciences, Geosciences and Biosciences Division, as part of the Computational Chemical Sciences Program at Pacific Northwest National Laboratory. Battelle operates the Pacific Northwest National Laboratory for the U.S. Department of Energy.

## ■ ABBREVIATIONS

MO, molecular orbitals; PEC, potential energy curves

## ■ REFERENCES

(1) Pauling, L. *The Nature of the Chemical Bond*, 3rd ed.; Cornell University Press: Ithaca, NY, USA, 1960; Chapter 1.

- (2) Lewis, G. N. The Atom and the Molecule. *J. Am. Chem. Soc.* **1916**, *38*, 762–785.
- (3) Walton, J. R.; Rivera-Rivera, L. A.; Lucchese, R. R.; Bevan, J. W. Is there any fundamental difference between ionic, covalent, and others types of bond? A canonical perspective on the question. *Phys. Chem. Chem. Phys.* **2017**, *19*, 15864–15869.
- (4) Leicester, H. M. Alexander Mikhailovich Butlerov. *J. Chem. Educ.* **1940**, *17*, 203–209.
- (5) Arbutov, B. A. 150th Anniversary of the birth of A. Bull. Acad. Sci. USSR, Div. Chem. Sci. **1978**, *27*, 1791–1794.
- (6) Roos, B. O.; Borin, A. C.; Gagliardi, L. Reaching the Maximum Multiplicity of the Covalent Chemical Bond. *Angew. Chem., Int. Ed.* **2007**, *46*, 1469–1472.
- (7) Nguyen, T.; Sutton, A. D.; Brynda, M.; Fettinger, J. C.; Long, G. J.; Power, P. P. Synthesis of a Stable Compound with Fivefold Bonding Between Two Chromium(I) Centers. *Science* **2005**, *310*, 844–847.
- (8) Shaik, S.; Danovich, D.; Wu, W.; Su, P.; Rzepa, H. S.; Hiberty, P. C. Quadruple Bonding in C<sub>2</sub> and Analogous Eight-Valence Electron Species. *Nat. Chem.* **2012**, *4*, 195–200.
- (9) Cheung, L. F.; Chen, T.-T.; Kocheril, G. S.; Chen, W.-J.; Czekner, J.; Wang, L.-S. Observation of Fourfold Boron-Metal Bonds in RhB(BO<sup>-</sup>) and RhB. *J. Phys. Chem. Lett.* **2020**, *11*, 659–663.
- (10) Grunenberg, J. Quadruply bonded carbon. *Nat. Chem.* **2012**, *4*, 154–155.
- (11) Shaik, S.; Rzepa, H. S.; Hoffmann, R. One Molecule, Two Atoms, Three Views, Four Bonds? *Angew. Chem., Int. Ed.* **2013**, *52*, 3020–3033.
- (12) Danovich, D.; Hiberty, P. C.; Wu, W.; Rzepa, H. S.; Shaik, S. The Nature of the Fourth Bond in the Ground State of C<sub>2</sub>: The Quadruple Bond Conundrum. *Chem. - Eur. J.* **2014**, *20*, 6220–6232.
- (13) Xu, L. T.; Dunning, T. H. Insights into the Perplexing Nature of the Bonding in C<sub>2</sub> From Generalized Valence Bond Calculations. *J. Chem. Theory Comput.* **2014**, *10*, 195–201.
- (14) Hermann, M.; Frenking, G. The Chemical Bond in C<sub>2</sub>. *Chem. - Eur. J.* **2016**, *22*, 4100–4108.
- (15) Shaik, S.; Danovich, D.; Braida, B.; Hiberty, P. C. The Quadruple Bonding in C<sub>2</sub> Reproduces the Properties of the Molecule. *Chem. - Eur. J.* **2016**, *22*, 4116–4128.
- (16) de Sousa, D. W. O.; Nascimento, M. A. C. Is There a Quadruple Bond in C<sub>2</sub>? *J. Chem. Theory Comput.* **2016**, *12*, 2234–2241.
- (17) Kharat, B.; Deshmukh, S. B.; Chaudhari, A. 4d Transition Metal Monoxides, Monocarbides, Monoborides, Mononitrides, and Monofluorides: A Quantum Chemical Study. *Int. J. Quantum Chem.* **2009**, *109*, 1103–1115.
- (18) Borin, A. C.; Gobbo, J. P. Electronic Structure and Chemical Bonding in the Lowest Electronic States of TcN. *J. Phys. Chem. A* **2009**, *113*, 12421–12426.
- (19) Scullman, R.; Thelin, B. The Spectrum of RuC in the Region 4100–4800 Å. *Phys. Scr.* **1972**, *5*, 201.
- (20) Lagerqvist, A.; Neuhaus, H.; Scullman, R. Das Bandenspektrum des RhC. *Z. Naturforsch., A: Phys. Sci.* **1965**, *20*, 751.
- (21) McIntyre, N. S.; Vander Auwera-Mahieu, A.; Drowart, J. Mass spectrometric determination of the dissociation energies of gaseous RuC, IrC and PtB. *Trans. Faraday Soc.* **1968**, *64*, 3006–3010.
- (22) Gingerich, K. A. Thermodynamic evidence for quadruple bond formation in the molecule ThRu and possible maximum bond energy between ligand-free metal atoms. *Chem. Phys. Lett.* **1974**, *25*, 523–526.
- (23) Scullman, R.; Thelin, B. The Spectrum of RuC in the Region 6 000–8700 Å. *Phys. Scr.* **1971**, *3*, 19–34.
- (24) Shim, I.; Finkbeiner, H. C.; Gingerich, K. A. Electronic States and Nature of Bonding of the RuC Molecule by All-Electron ab Initio HF-CI Calculations and Equilibrium Mass Spectrometric Experiments. *J. Phys. Chem.* **1987**, *91*, 3171–3178.
- (25) DaBell, R. S.; Meyer, R. G.; Morse, M. D. Electronic structure of the 4d transition metal carbides: Dispersed fluorescence spectroscopy of MoC, RuC, and PdC. *J. Chem. Phys.* **2001**, *114*, 2938–2954.
- (26) Langenberg, J. D.; DaBell, R. S.; Shao, L.; Dreessen, D.; Morse, M. Resonant two-photon ionization spectroscopy of jet-cooled RuC. *J. Chem. Phys.* **1998**, *109*, 7863–7875.
- (27) Shim, I.; Gingerich, K. A. Electronic structure and bonding in the monocarbides in the first platinum metal triad. *Surf. Sci.* **1985**, *156*, 623–634.
- (28) Shim, I.; Gingerich, K. A. All-electron ab initio investigations of the three lowest-lying electronic states of the RuC molecule. *Chem. Phys. Lett.* **2000**, *317*, 338–345.
- (29) Guo, R.; Balasubramanian, K. Spectroscopic properties and potential energy curves of low-lying electronic states of RuC. *J. Chem. Phys.* **2004**, *120*, 7418–7425.
- (30) Steimle, T. C.; Virgo, W. L.; Brown, J. M. Permanent electric dipole moments and hyperfine interaction in ruthenium monocarbide, RuC. *J. Chem. Phys.* **2003**, *118*, 2620.
- (31) Virgo, W. L.; Steimle, T. C.; Aucoin, L. E.; Brown, J. M. The permanent electric dipole moments of ruthenium monocarbide in the 3Π and 3Δ states. *Chem. Phys. Lett.* **2004**, *391*, 75–80.
- (32) Wang, J.; Sun, X.; Wu, Z. Chemical bonding and electronic structure of 4d-metal monocarbides. *Chem. Chem. Phys. Lett.* **2006**, *426*, 141–147.
- (33) Lindholm, N. F.; Hales, D. A.; Ober, L. A.; Morse, M. D. Optical spectroscopy of RuC: 18000–24000 cm<sup>-1</sup>. *J. Chem. Phys.* **2004**, *121*, 6855–6860.
- (34) Wang, F.; Steimle, T. C.; Adam, A. G.; Cheng, L.; Stanton, J. F. The pure rotational spectrum of ruthenium monocarbide, RuC, and relativistic ab initio predictions. *J. Chem. Phys.* **2013**, *139*, 174318.
- (35) Auwera-Mahieu, A. V.; Peeters, R.; McIntyre, N. S.; Drowart, J. Mass Spectrometric Determination of Dissociation Energies of the Borides and Silicides of some Transition Metals. *Trans. Faraday Soc.* **1970**, *66*, 809–816.
- (36) Chowdhury, P. K.; Balfour, W. J. A spectroscopic characterization of the electronic ground state of rhodium monoboride. *J. Chem. Phys.* **2006**, *124*, 216101.
- (37) Merriles, D. M.; Tieu, E.; Morse, M. D. Bond dissociation energies of FeB, CoB, NiB, RuB, RhB, OsB, IrB, and PtB. *J. Chem. Phys.* **2019**, *151*, 044302.
- (38) Chowdhury, P. K.; Balfour, W. J. A spectroscopic study of the rhodium monoboride molecule. *Mol. Phys.* **2007**, *105*, 1619–1624.
- (39) Borin, A. C.; Gobbo, J. P. Low-Lying Singlet and Triplet Electronic States of RhB. *J. Phys. Chem. A* **2008**, *112*, 4394–4398.
- (40) Prascher, B. P.; Woon, D. E.; Peterson, K. A.; Dunning, T. H.; Wilson, A. K. Gaussian basis sets for use in correlated molecular calculations VII. Valence, core-valence, and scalar relativistic basis sets for Li, Be, Na, and Mg. *Theor. Chem. Acc.* **2011**, *128*, 69–82.
- (41) Dunning, T. H. Gaussian basis sets for use in correlated molecular calculations. I. The atoms boron through neon and hydrogen. *J. Chem. Phys.* **1989**, *90*, 1007–1023.
- (42) Kendall, R. A.; Dunning, T. H.; Harrison, R. J. Electron affinities of the first-row atoms revisited. Systematic basis sets and wave functions. *J. Chem. Phys.* **1992**, *96*, 6796–6806.
- (43) Peterson, K. A.; Figgen, D.; Dolg, M.; Stoll, H. Energy-consistent relativistic pseudopotentials and correlation consistent basis sets for the 4d elements Y-Pd. *J. Chem. Phys.* **2007**, *126*, 124101.
- (44) Werner, H. - J.; Knowles, P. J. An efficient internally contracted multiconfiguration-reference configuration interaction method. *J. Chem. Phys.* **1988**, *89*, 5803–5814.
- (45) Langhoff, S. R.; Davidson, E. R. Configuration interaction calculations on the nitrogen molecule. *Int. J. Quantum Chem.* **1974**, *8*, 61–72.
- (46) Knowles, P. J.; Hampel, C.; Werner, H.-J. Coupled cluster theory for high spin, open shell reference wave functions. *J. Chem. Phys.* **1993**, *99*, 5219–5227.
- (47) Langhoff, S. L.; Bauschlicher, C. W., Jr.; Partridge, H. Theoretical dipole moment for the X<sup>2</sup>Π state of NO. *Chem. Phys. Lett.* **1994**, *223*, 416–422.
- (48) Tzeli, D.; Mavridis, A. On the dipole moment of the ground state X<sup>3</sup>Δ of iron carbide, FeC. *J. Chem. Phys.* **2003**, *118*, 4984–4986.
- (49) Tzeli, D.; Mavridis, A. Theoretical investigation of iron carbide, FeC. *J. Chem. Phys.* **2002**, *116*, 4901–4921 (2002)..
- (50) Tao, M.; Perdew, J. P.; Staroverov, V. N.; Scuseria, G. E. Climbing the density functional ladder: Nonempirical meta-generalized

gradient approximation designed for molecules and solids," *Phys. Phys. Rev. Lett.* **2003**, *91*, 146401.

(51) Frisch, M. J.; Trucks, G. W.; Schlegel, H. B.; Scuseria, G. E.; Robb, M. A.; Cheeseman, J. R.; Scalmani, G.; Barone, V.; Petersson, G. A.; Nakatsuji, H.; et al. *Gaussian 16*, Revision A.01; Gaussian: Wallingford, CT, USA, 2016.

(52) Werner, H.-J.; Knowles, P. J.; Knizia, G.; Manby, F. R.; Schütz, M.; Celani, P.; Gyröffy, W.; Kats, D.; Korona, T.; Lindh, R. et al. *MOLPRO Quantum Chemistry Software*, v. 2012.1 (package of ab initio programs).

(53) (a) Technetium (Tc). *Basic Spectroscopic Data*; National Institute of Standards and Technology, <https://physics.nist.gov/PhysRefData/Handbook/Tables/technetiumtable6.htm> (Accessed August 5, 2020). (b) *Handbook of Basic Atomic Spectroscopic Data*, NIST Standard Reference Database 108; National Institute of Standards and Technology, <https://physics.nist.gov/PhysRefData/Handbook/Tables/rutheniumtable6.htm> (Accessed August 5, 2020).

(c) Rhodium (Rh). *Basic Spectroscopic Data*; National Institute of Standards and Technology, <https://physics.nist.gov/PhysRefData/Handbook/Tables/rhodiumtable6.htm> (Accessed August 5, 2020).

(d) Palladium (Pd). *Basic Spectroscopic Data*; National Institute of Standards and Technology, <https://physics.nist.gov/PhysRefData/Handbook/Tables/palladiumtable6.htm> (Accessed August 5, 2020).

(54) Tzeli, D.; Mavridis, A. Accurate ab initio calculations of the ground states of FeC, FeC<sup>+</sup>, and FeC<sup>-</sup>. *J. Chem. Phys.* **2010**, *132*, 194312.

(55) Steimle, T. C.; Virgo, W. L.; Hostutler, D. A. The permanent electric dipole moments of iron monocarbide, FeC. *J. Chem. Phys.* **2002**, *117*, 1511–1516.

(56) Balfour, W. I.; Cao, J.; Prasad, C. V. V.; Qian, C. X. W. *J. Chem. Phys.* **1995**, *103*, 4046.

(57) Jensen, W. B. Electronegativity from Avogadro to Pauling: Part 1: Origins of the Electronegativity Concept. *J. Chem. Educ.* **1996**, *73*, 11.

(58) Tzeli, D.; Mavridis, A. Electronic structure and bonding of the 3d-transition metal borides, MB, M = Sc, Ti, V, Cr, Mn, Fe, Co, Ni, and Cu through all electron ab initio calculations. *J. Chem. Phys.* **2008**, *128*, 034309.